Published in final edited form as:
Transl Res. 2018 March ; 193: 13–30. doi:10.1016/j.trsl.2017.10.008.

Development of mannose functionalized dendrimeric nanoparticles for targeted delivery to macrophages: use of this platform to modulate atherosclerosis

HONGLIANG HE, **QUAN YUAN**, **JINGHUA BIE**, **RYAN L. WALLACE**, **PAUL J. YANNIE**, **JING WANG**, **MICHAEL G. LANCINA III**, **OLGA YU ZOLOTARSKAYA**, **WILLIAM KORZUN**, **HU YANG**, and **SHOBHA GHOSH**

Dept. of Chemical and Life Science Engineering, Virginia Commonwealth University (VCU), Richmond, Va; Dept. of Internal Medicine, VCU Medical Center, Richmond, Va; Hunter Homes McGuire VA Medical Center, Richmond, Va; Dept. of Biomedical Engineering, VCU, Richmond, Va; Dept. of Clinical and Laboratory Sciences, VCU Medical Center, Richmond, Va; Dept. of Pharmaceutics, VCU, Richmond, Va; Massey Cancer Center, VCU Medical Center, Richmond, Va.

Abstract

Dysfunctional macrophages underlie the development of several diseases including atherosclerosis where accumulation of cholesteryl esters and persistent inflammation are 2 of the critical macrophage processes that regulate the progression as well as stability of atherosclerotic plaques. Ligand-dependent activation of liver-x-receptor (LXR) not only enhances mobilization of stored cholesteryl ester but also exerts anti-inflammatory effects mediated via trans-repression of proinflammatory transcription factor nuclear factor kappa B. However, increased hepatic lipogenesis by systemic administration of LXR ligands (LXR-L) has precluded their therapeutic use. The objective of the present study was to devise a strategy to selectively deliver LXR-L to atherosclerotic plaque-associated macrophages while limiting hepatic uptake. Mannose-functionalized dendrimeric nanoparticles (mDNP) were synthesized to facilitate active uptake via the mannose receptor expressed exclusively by macrophages using polyamidoamine dendrimer. Terminal amine groups were used to conjugate mannose and LXR-L T091317 via polyethylene glycol spacers. mDNPLXR-L was effectively taken up by macrophages (and not by hepatocytes), increased expression of LXR target genes (ABCA1/ABCG1), and enhanced cholesterol efflux. When administered intravenously to LDLR−/− mice with established plaques, significant accumulation of fluorescently labeled mDNP-LXR-L was seen in atherosclerotic plaque-associated macrophages. Four weekly injections of mDNP-LXR-L led to significant reduction in atherosclerotic plaque progression, plaque necrosis, and plaque inflammation as assessed by expression of nuclear factor kappa B target gene matrix metalloproteinase 9; no increase in hepatic lipogenic genes or plasma lipids was observed. These studies validate the development of a macrophage-specific delivery platform for the delivery of anti-atherosclerotic agents directly to the plaque-associated macrophages to attenuate plaque burden.

Reprint requests: Shobha Ghosh, Department of Internal Medicine, VCU Medical Center, Richmond, VA 23298; shobha@vcu.edu.

INTRODUCTION

Macrophages are effector cells that not only play a major role in innate and adaptive immunity, but also play an important role in tissue repair and homeostasis. However, normal physiological functions of macrophages are perturbed in several diseases including metabolic diseases such as atherosclerosis, diabetes, and obesity. Therefore, targeting the recruitment, activation, or regulation of dysfunctional macrophages represents a promising therapeutic strategy. With the advancement of nanotechnology, development of nanomedicines to efficiently target dysfunctional macrophages can strengthen the effectiveness of therapeutics and improve clinical outcomes.[1] Several macrophage-specific surface receptors have been described including mannose receptor,[2] folate receptor,[3] and TIM-4 or BAI-1[4,5] that can potentially be used for effective targeting. Although folate-functionalized nanomedicine to target cancerous tissue-associated macrophages has been described[6]; strategies to target dysfunctional macrophages in other chronic diseases such as atherosclerosis are very limited.

Among the vast repertoire of nanomedicine options, polyamidoamine (PAMAM) dendrimers offer several distinct advantages for the development of multifunctional dendrimeric nanoparticles (DNP). More than 120 terminal amine groups on PAMAM dendrimer generation 5.0 permit accessible surface modifications and also offer high buffering capacity for the unique “proton-sponge” effect desirable for endosomal escape. Furthermore, PEGylation of DNP prevents agglomeration, decreases the highly positive charge on the surface, and increases the high steric exclusion, thus extending the circulation time in the blood.[7–9] We have successfully developed several PAMAM-derived nanoparticles and demonstrated their use for enhanced delivery of drugs[10] as well as for gene delivery.[11] Furthermore, functionalized PAMAM dendrimer-triglycine-Epidermal growth factor nanoparticles were demonstrated to successfully deliver drugs or nucleic acids via specific receptor binding.[12] Thus, PAMAM dendrimer-based DNPs represent a viable starting point to develop nanomedicines to target dysfunctional macrophages.

Atherosclerosis is one of the many metabolic diseases where dysfunctional macrophages play a causal role and are involved in all stages of its development. The 2 main and causally related characteristics of the dysfunctional macrophages in atherosclerosis are accumulation of cholesteryl esters (CE) and inability to appropriately resolve inflammation.[13,14] Intracellular CE accumulation in macrophages can be reduced by enhancing the removal of unesterified or free cholesterol (FC), a process rate-limited by intracellular CE hydro-lysis catalyzed by neutral CE hydrolase (CEH),[15,16] and earlier studies from our laboratory have demonstrated CEH overexpression-mediated increase in CE mobilization.[17–19] FC generated by CEH-mediated hydrolysis of CE becomes available for ApoA1 or High density lipoprotein-dependent efflux through FC transporters ABCA1/G1[20] and carried to the liver for final elimination from the body. Although overexpression of ABCA1 attenuates atherosclerosis,[21,22] deficiency of ABCA1 in macrophages enhances plaque progression.[23] Therefore, a strategy to enhance FC removal from dys-functional macrophage foam cells by simultaneously increasing CEH activity[24] and ABCA1/G1 expression[25] is likely to attenuate foam cell formation. Activation of liver-X-receptor (LXR) is one such strategy. LXR activation in macrophages is athero-protective,[25,26] and the underlying mechanism is

thought to be increased expression of ABCA1/G1 resulting in increased FC efflux from macrophage foam cells. Functional LXR response elements are also present in the proximal CEH promoter and LXR-L increase CEH promoter activity.[27] Therefore, targeted delivery of LXR-L to macrophages will potentially increase FC efflux by modulating 2 critical intracellular mechanisms. Ligand-mediated activation of LXR also suppresses inflammation via trans-repression of nuclear factor kappa B (NF-κB)-mediated inflammatory pathways.[28] Consistently, administration of an LXR agonist results in attenuation of atherosclerosis in LDLR−/− and ApoE−/−[29] mice, and macrophage LXR are considered as endogenous inhibitors of atherosclerosis.[30] Despite these promising effects, the use of LXR-L in clinical arena is hindered by the observed hepatic steatosis (>6-fold increase in liver triglycerides [TGs]) and hypertriglyceridemia (>2-fold increase) because of activation of hepatic LXR.[31] In the liver, LXR acts as a master lipogenic transcription factor to directly regulate fatty acid synthase (FAS) and sterol regulatory element-binding protein 1 ([SREBP1] a prolipogenic transcription factor), thus enhancing lipogenesis.[32] Hence, to maximize the efficacy of LXR-L in treatment of atherosclerosis, it is essential to devise a strategy to selectively deliver LXR-L to atherosclerotic plaque-associated macrophages while limiting its hepatocyte uptake.

The present study was therefore undertaken to develop such a functionalized DNP-based platform for specific delivery of payloads to macrophages. Advantage was taken of the specific surface expression of mannose receptor on macrophages to develop mannose functionalized DNP (mDNP) for targeted delivery of LXR-L to macrophages. Data presented herein demonstrate the suitability of mDNP for specific delivery of LXR-L to macrophages and not to hepatocytes, thereby eliminating the undesirable lipogenic effects in the liver. Furthermore, the data also show that targeted delivery of LXR-L to athero-sclerotic plaques-associated macrophages results in LXRL-dependent plaque attenuation and favorable modulation of plaque characteristics.

MATERIALS AND METHODS

Materials.

Ethylenediamine core PAMAM dendrimer generation 5.0 (technical grade) was purchased from Dendritech (Midland, MI). Fluorescein isothiocyanate (FITC), 4-nitrophenyl chloroformate (NPC), triethylamine, COOH-polyethylene glycol (PEG)-NH_2 (M_n = 3500 g/mol), tetrahydrofuran, 1-ethyl-3-(−3-dimethylaminopropyl) carbodiimide hydrochloride, N-hydroxysuccinimide (NHS), and LXR-L T0901317 were purchased from Sigma-Aldrich (St. Louis, MO). Mannose-PEG-NHS (M_n = 3500 g/moL) was custom synthesized by JenKem Technology (Plano, TX). Near infrared dye 800CW-NHS ester was obtained from Li-COR Biotechnology (Lincoln, NE). SnakeSkin dialysis tubing with 3500 molecular weight cutoff (MWCO) was purchased from Thermo Scientific (Rockford, IL). William's E medium, Dulbecco's Modified Eagle's Medium medium, fetal bovine serum (FBS), and Dulbecco's phosphate-buffered saline (DPBS) were obtained from Gibco BRL (Carlsbad, CA). Trypsin-EDTA (0.25%), streptomycin, and penicillin were obtained from Invitrogen Co. Vectashield mounting media were purchased from Vector Laboratories (Burlingame, CA). RNeasy Mini Kit was purchased from QIAGEN. High-capacity cDNA Reverse Transcription Kit and

TaqMan Universal PCR Master Mix, no AmpErase UNG were obtained from Applied Biosystems. All other chemicals were purchased from Sigma-Aldrich.

Synthesis and characterization of functionalized DNP.

The overall synthesis scheme is shown in Fig 1, A. In brief, 5 mg of LXR-L (10 mg/mL in DMSO as stock solution) and COOH-PEG-NH_2 (the molar ratio of PEG to LXR-L was 1:1.05) was mixed in 10 mL of tetrahydrofuran and stirred overnight in the presence of NPC (the molar ratio of PEG to NPC was 1:1.5) and excess triethylamine. The reaction product was filtered, and the solvent was evaporated under vacuum. The obtained residue was dissolved in water, subjected to dialysis with 3000 MWCO overnight and then lyophilized to obtain COOH-PEG-LXR-L. COOH-PEG-LXR-L was coupled to the amino groups on the surface of PAMAM dendrimer G5.0 in DMSO via the 1-ethyl-3-(−3-dimethylaminopropyl) carbodiimide hydrochloride-NHS reaction. Following an overnight incubation, the solvent was dialyzed by water to remove the DMSO and lyophilized to obtain DNP-LXR-L. The DNP-LXR-L was dissolved in 0.1 M sodium bicarbonate solution and mannose-PEG-NHS was added (the molar ratio of mannose-PEG-NHS to G5 was approximately 10:1). The resulting mixture was stirred overnight at room temperature followed by sufficient dialysis with 3000 MWCO and lyophilization to get the final product mDNP-LXR L. To facilitate monitoring of intracellular uptake and trafficking, FITC was coupled to mDNP-LXR-L or G5 as described earlier.[33] To monitor the specific targeting to macrophages in atherosclerotic plaques, Near infrared (NIR) dye 800CW-NHS ester was coupled to the mDNP-LXR-L based on the procedure described before.[34] ^{1}H NMR spectra were recorded on a Varian superconducting Fourier-transform NMR spectrometer (Mercury-300).[35] D_2O was used as the solvent. The proton chemical shift of D_2O is 4.8 ppm. The particles used in this study were DNP (PAMAM G5.0), mDNP (mannose functionalized DNP), and mDNP-LXR-L (mannose functionalized DNP conjugated to LXR-L T0901317). Particle size and zeta potential information was obtained by using a Malvern Zetasizer Nano ZS90 apparatus (Malvern Instruments, Worcestershire, UK). Changes in the size and zeta potential of mDNP-LXR-L were also monitored during 24-hour incubation at 37°C to test its colloidal stability after re-suspension in DPBS.

In vitro validation.

Cell culture.—Thioglycollate-elicited mouse peritoneal macrophages (MPMs) were harvested, and non-adherent cells were removed after 4 hours, and medium was replaced with fresh growth medium (10% FBS containing Dulbecco's Modified Eagle's Medium medium).[24] Primary mouse hepatocytes were prepared as described earlier.[36] Cells (0.7×10^6 cells/well) were plated in collagen-coated 6-well plates, and the growth medium (William's E medium without phenol red containing hepatocyte thawing as well as plating supplement from Invitrogen) was changed after 3 hours. After 24 hours, the medium was replaced with fresh medium.

Mannose receptor expression.—The mannose receptor expression was examined in macrophages or hepatocytes by Western blot analyses. Briefly, cells were washed twice with ice-cold DPBS, and then lysed by incubating in the RIPA buffer supplemented with protease and phosphatase inhibitor cocktail (Sigma-Aldrich) for 30 minutes at 4°C. The

proteins (~30 μg) were separated by 10% SDS-PAGE (Bio-Rad Laboratories), transferred to polyvinylidene difluoride membrane, immunoblotted with 1:200 diluted anti-mannose receptor rabbit polyclonal antibody (ab64693, Abcam, Cambridge, MA) and followed by goat anti-rabbit antibody conjugated to IRDye 800 CW (green). Positive immunoreactivity was detected using the Odyssey CLx imaging system. The membrane was stripped and re-probed for actin using mouse monoclonal antibody (sc-47778, Santa Cruz Biotechnology) and goat anti-mouse secondary antibody conjugated to IRDye 680CW (red).

Evaluation of cell viability following mDNP-LXR-L uptake.—Freshly isolated MPMs (0.8×10^6 cells/well) or mouse hepatocytes (0.3×10^6 cells/well) were plated in 48-well plates, and growth medium was changed after 4 hours. After 24 hours, the growth medium was replaced with fresh medium containing increasing concentrations of mDNP-LXR-L and incubated for an additional 24 hours. Cell viability was determined using WST-1 assay.

Cellular uptake of mDNP by macrophages or hepatocytes.—For imaging of mDNP uptake, cells were plated in 2-well chamber slides. At the end of each treatment, cells were washed with DPBS, fixed with 4% formaldehyde at room temperature for 20 minutes, permeabilized with 0.1% Triton X-100 for 5 minutes, and the cell nuclei were counterstained with 4', 6-diamino-2-phenylindole (DAPI) for 5 minutes. Cellular uptake was assessed by fluorescent imaging, a 405 nm laser line was selected for DAPI, and a 488 nm laser line was selected for FITC. For quantification of uptake, cells were harvested at the end of the incubation, analyzed by flow cytometry, and uptake of mDNP was expressed as mean fluorescence intensity. To evaluate the specificity of mDNP uptake by macrophages, MPMs were pretreated with 0.1 mM mannan (mannose receptor antagonist) for 30 minutes before the addition of 0.2 μM mDNP-FITC.

CEH activity.—Intracellular CEH activity was measured by monitoring the hydrolysis of cholesteryl [1-^{14}C] oleate. The substrate was presented as micelles and was prepared as described by Hajjar et al.[37] In a standard assay, 25 μL of this substrate was used in a final volume of 500 μL, giving the final concentration of 6 μM cholesteryl oleate, 23.7 μM phosphatidyl choline, and 12.5 μM sodium taurocholate. CE hydrolytic activity was measured using 3 different protein concentrations to ensure linearity, and each assay was performed in duplicate. The activity is expressed as nmoles of [1-^{14}C] oleate released/h/mg protein.[38]

FC efflux assays.—Freshly isolated MPMs (1×10^6 cells/well) were plated in 24-well culture plates and incubated overnight. The intracellular FC and CE pools were labeled with [^{3}H]-cholesterol by incubating the cells for 48 hours with serum-free medium containing 1 μCi/mL [^{3}H]-cholesterol (Perkin Elmer) and 25 μg/mL acetylated LDL (Kalen Biomedical, Inc). The cells were then washed and incubated with serum-free medium for 24 hours to allow all pools of cholesterol to equilibrate. Following equilibration, FC efflux was initiated by replacing the medium with growth medium containing 10% FBS, and % FC efflux was determined as described earlier.[18]

In vivo validation.

All animal procedures were approved by the Institutional Animal Care and Use Committee of Virginia Commonwealth University and conform to the relevant ethical guidelines for animal research. LDL receptor knockout mice (LDLR−/−) originally obtained from Jackson Laboratory and maintained in the laboratory in a barrier facility were used for all studies. At 10 weeks of age, mice of both sexes were fed a high-fat, high-cholesterol Western-type diet (WD, TD88137, Harlan Teklad), which contained 21% fat, 0.15% cholesterol, and 19.5% casein by weight with no sodium cholate for 12 weeks. After 12 weeks, the mice were switched to chow diet. The experimental group was injected (i.v., weekly for 4 weeks) with mDNP-LXR-L (200 μg in 100 μL DPBS), and the control group did not receive any injections. It should be noted that strong in vitro and in vivo data demonstrating no effects of mDNP in modulating LXR target gene expression in macrophages or liver precluded the necessity to inject control mice with mDNP alone. Following an overnight fast, the mice were euthanized (by inhalation of isoflurane) to collect blood, aorta, and heart for analyses.

Uptake of mDNP by atherosclerotic plaque-associated macrophages.—To image the uptake of mDNP by atherosclerotic plaque-associated macrophages in vivo, NIR-mDNP (labeled with 800CW) were injected (i.v., 0.25 mg 800CW/kg, 3 mice per group) into LDLR−/− mice with established atherosclerotic lesions as a result of WD feeding for 16 weeks. For ex vivo imaging, the major organs (heart, liver, spleen, lung, and kidney, as well as the entire aorta) were harvested after 24 hours and imaged using Odyssey Fc Imaging System (LI-COR, Lincoln, NE) at ex/em = 780/800 nm. To quantify the uptake by the macrophages associated with the aortic lesions, mDNP-FITC was injected into 16-week-old atherosclerotic mice (0.5 mg FITC/kg, 3 mice per group). Aortic arch was dissected, cleaned, and digested as described by Galkina et al[39] and used in our laboratory.[40] Isolated cells were re-suspended in Fluorescence activated cell sorting buffer containing Fc block and incubated with fluorescently labeled anti-CD45 antibody (CD45-PE, eBioscience) and anti-CD11b antibody (CD11b-AlexaFluor 700, eBioscience) for 20 minutes at 4°C. After washing, specific immunofluorescent staining of individual cells in the total cell suspension was detected by flow cytometry (BD Biosciences, Canto II) and the data were analyzed using FlowJO software (Tree Star Inc.). Uptake of mDNP-FITC was quantified by determining the mean fluorescent intensity of FITC in CD11b+ macrophages in the CD45+ population. To evaluate retention of CD11b+FITC+ cells in the atherosclerotic plaques following a single injection, data were expressed as %CD11b+FITC+ cells at given time.

Expression of LXR-target genes.—Total RNA (from MPMs, hepatocytes, or liver) was extracted with RNeasy Mini Kit (Qiagen, Valencia, CA). Five microgram of total RNA was reverse transcribed with Thermoscript RTPCR System (Invitrogen), and first-strand cDNA was used to perform real-time PCR using Stratgene Mx3000p real-time PCR system with TaqMan Gene Expression Assays for ABCA1 (Mm00442646_m1), ABCG1 (Mm00437390_m1), FAS (Mm00662319_m1), and SREBP1 (Mm00550338_m1) (Applied Biosystems, Foster City, CA).

Plasma analyses.—Total plasma cholesterol, TGs, liver enzymes aspartate transaminase and alanine transaminase, as well as blood urea nitrogen (BUN) and creatinine were

determined using the Cobas c311 automated chemistry analyzer with reagents, calibrators, and controls from Roche Diagnostics. Interleukin-6 levels were determined using Ready-set-Go ELISA kit from eBioscience.

Quantitative atherosclerosis analyses.—The aorta was dissected from the heart to the iliac bifurcation, cleaned of any surrounding tissue, opened longitudinally, pinned on black wax, and fixed for 24 hours in 10% buffered formalin. The fixed aortas were imaged on a black background using a Canon Digital Camera fitted with a 60 mm, f/2.8 Macro Lens. Total area and the area occupied by the lesions in the aortic arch as well as total aorta was determined using Axiovision Image Analysis software (Carl Zeiss).[24]

Morphological analyses of the lesions.—Hearts were fixed in buffered formalin, paraffin embedded and sectioned. Once the aortic sinus was visible, serial sections (5-m thick) were transferred to numbered slides. Serially numbered slides were then stained with Masson trichrome stain and hematoxylin-eosin. Images were acquired with Zeiss Observer A1 inverted microscope and analyzed by Axiovision Image Analysis Software to quantify the total lesion or % necrotic area.[24]

Immunohistochemistry.—Heart sections (2 per slide) with visible aortic root were dewaxed using CitraSolv and rehydrated using serial incubations in 100%, 95%, and 70% ethanol followed by deionized water. Following antigen retrieval in preheated citrate buffer (10 mM sodium citrate, 0.05% Tween 20, pH 6.0, 95°C), the sections were incubated with 5% horse serum (blocking solution) to block nonspecific sites. The sections were subsequently incubated overnight with either primary antibody (negative control) or anti-matrix metalloproteinase 9 (MMP-9) antibody (sc-6840, goat polyclonal antibody, 1:50 dilution in blocking solution). Following 3 washes in PBS, sections were then incubated with biotin-conjugated horse anti-goat IgG for 1 hour followed by NeutrAvidin-conjugated Alexa Flour546 as the fluorescent detection reagent. Cover-slips were mounted using ProLong Diamond antifade mountant with DAPI (Molecular Probes). Images were acquired using a Zeiss inverted microscope fitted with a digital camera in a multi-acquisition mode using pseudo-coloring.

Statistical analysis.

All data were analyzed using GraphPad Prism software. Statistical significance of difference between groups was determined by analysis of variance, and Tukey multiple comparison tests were performed to evaluate the significant difference between groups, if applicable. $P < 0.05$ was considered statistically significant.

RESULTS

Synthesis and characterization of mDNP-LXR-L.

Fig 1, A, details the steps involved in the synthesis of mDNPLXR-L using PAMAM dendrimer G5.0 as a polymeric core, LXR-L T0901317 as the model drug, and mannose-PEG-NHS as a targeting ligand. PEG spacer between LXR-L and PAMAM G5.0 as well as mannose and PAMAM G5.0 was added to achieve a longer circulation time in blood.

Following the synthesis, the final product mDNP-LXR-L was purified by sufficient dialysis and characterized for its physiochemical properties. ^{1}H NMR spectrum (Fig 1, B) shows that the final product has relatively high purity without interfering proton peaks from the reactants, intermediates, or reaction solvent. The methylene protons of branching units within the dendrimer have multiple peaks between 2.2 and 3.4 ppm. The methylene protons of repeat units from mannose-PEG and PEGLXR-L have a singlet peak at 3.6 ppm. The proton peaks between 6.5 and 7 ppm are attributed to the benzene ring protons of LXR-L. Based on the integrals of the proton peaks, the stoichiometric ratio for PEG-LXR-L:PEG-mannose-NHS:G5.0 was approximately 5:10:1. The particles had a relatively uniform size as seen in Fig 1, C. The surface functionalization chemistry did not noticeably change the size of DNPs. The mean hydrodynamic size of mDNP-LXR-L was ~5 nm with a narrow polydispersity (Fig 1, D), consistent with the reported value of commercially available PAMAM dendrimer G5.0. The zeta potential of mDNP-LXR-L decreased from ~30 mV (unmodified PAMAM dendrimer G5.0) to ~6 mV (zero time point, data not shown) and did not change over time (Fig 1, E), suggesting that the PEGylation significantly shielded the positively charged dendrimer surface. Colloidal stability tests also showed that mDNP-LXR-L had excellent stability with no obvious change in size (Fig 1, F) over the 24-hour time period tested.

In vitro validation.

Evaluation of cellular toxicity.—Mouse hepatocytes or MPMs were exposed to increasing concentrations of mDNP-LXR-L, and cell viability was evaluated. As shown in Fig 2, A, no significant decrease in cell viability was noted in MPMs even when exposed to a concentration of 2 μM. However, a decrease in cell viability was noted when hepatocytes (Fig 2, B) were exposed to concentrations above0.2 μM.

Specificity of uptake by macrophages.—Activation of LXR in hepatocytes leads to an undesirable increase in lipogenic target genes,[31] leading to increased hepatic lipid accumulation. The foremost objective of the present study was to develop a platform with specific delivery to macrophages and yet limited the uptake by hepatocytes. For targeted delivery of DNP to macrophages, advantage was taken of the specific expression of mannose receptor on macrophages. As shown in Fig 3, A, mannose receptor was highly expressed on MPMs (labeled as MΦ) and negligible expression was seen in hepatocytes. Consistently, macrophages showed higher uptake of mDNP-FITC compared with primary mouse hepatocytes (Fig 3, B), and significantly higher mean fluorescent intensity of FITC was associated with macrophages compared with hepatocytes (1070.2 ± 99.8 vs 310.3 ± 45.2, $P < 0.001$, n = 6) (Fig 3, C), validating the specificity imparted by mannose functionalization of DNP. It is noteworthy that in addition to macrophages, mannose receptors are also expressed on immature dendritic cells where they mediate high efficiency uptake of glycosylated antigens.[41]Being phagocytic in nature, macrophages are likely to nonspecifically take up DNP, and the ability of mannose functionalization to impart specificity was further tested by comparing concentration-dependent uptake of DNP-FITC and mDNP-FITC by MPMs. A concentration-dependent increase in uptake of DNP was noted and at all concentrations tested; uptake of mDNP-FITC was higher than that seen for DNP-FITC (Fig 4, A). Using 0.2 μM as the optimized concentration, DNP uptake kinetics

was evaluated. Not only was the uptake time-dependent, increased uptake of mDNP-FITC was also noted at all time points compared with DNP-FITC (Fig 4, B), demonstrating specific macrophage targeting by mannose functionalization of DNP. Based on the observed fluorescent intensities, maximum uptake was noted by 24 hours and it was indistinguishable with that seen at 48 hours. More importantly, no morphological changes were noted, and cell viability remained unchanged with time. Specificity of uptake of mDNPFITC by MPMs was further confirmed by evaluating the uptake in cells pretreated with mannose receptor antagonist mannan. Significant reduction in mDNP-FITC by MPMs exposed to mannan (Fig 4, C) further demonstrated the specificity of mDNP uptake by macrophages via the mannose receptor.

Intracellular functionality of LXR-L (T0901317) when delivered using mDNP-LXR-L.—With the primary objective to develop a macrophage-specific delivery platform with limited or negligible delivery to hepatocytes, we next tested the ability of mDNP-LXR-L to activate LXR in MPMs and increase the expression of LXR-target genes (eg, ABCA1 and ABCG1). As shown in Fig 5, A compared with untreated controls or mDNP alone, significant increase in ABCA1 and ABCG1 expression was noted when MPMs were treated with mDNP-LXR-L. Furthermore, this LXR-mediated increase in gene expression was comparable with that seen with MPMs treated with free LXR-L. In contrast, as shown in Fig 5, B mDNP-LXR-L failed to increase the expression of LXR-target genes (eg, FAS and SREBP1) in hepatocytes while exposure of hepatocytes to free LXR-L led to significant increase in the expression of FAS and SREBP1. To further examine the functional consequences of LXR-L-dependent increase in gene expression, cellular CEH activity was monitored. mDNP-LXR-L delivered LXR-L significantly increased CEH activity compared with MPMs treated with mDNP alone (Fig 5, C). This increase in CEH activity by mDNP-LXR-L was comparable with that observed by directly treating the MPMs with free ligand, indicating that mDNP-LXR-L delivered ligand is equally effective. The potential therapeutic use of developing a macrophage-specific platform is to be able to facilitate the removal of stored CE from macrophage foam cells in an effort to reduce atherosclerotic plaque burden. Therefore, to further examine if mDNP-LXR-L mediated increase in ABCA1/ABCG1 expression as well as increase in CEH activity leads to an increase in FC removal from MPMs, FC efflux was monitored. Significantly higher FC efflux was observed from MPMs treated with mDNP-LXR-L compared with those treated with mDNP (Fig 5, D) at both time points tested. Furthermore, this increase in FC efflux was comparable with that seen in MPMs directly treated with free LXR-L, demonstrating the efficacy or functionality of LXR-L delivered by mDNP-LXR-L.

In vivo validation.

Uptake of mDNP by atherosclerotic plaque-associated macrophages.—To evaluate delivery of payloads to atherosclerotic plaques, initial experiments compared the uptake of intravenously administered DNP or mDNP conjugated to NIR dye 800CW by different tissues including the aorta. Ex vivo imaging of the dissected aorta was performed to monitor uptake of DNP by plaque-associated macrophages. Considerable increase in uptake of mDNP compared with nonfunctionalized DNP was noted in the isolated aortic tree (Fig 6, A, Top Panel). It is noteworthy that macrophage-rich tissues such as liver, kidney, lung, and

spleen also show uptake of NIR-DNP consistent with uptake by resident macrophages in these tissues (Fig 6, A, Middle and Bottom Panels). Although mannose functionalization in NIR-mDNP-LXR-L did not affect the uptake by these tissues, significant increase in uptake was observed only in the aorta (Fig 6, B). Furthermore, mannose functionalization significantly reduced the clearance by kidney probably because of the surface modification of DNP by mannose and PEG spacer. To specifically determine the uptake by arterial plaque-associated macrophages, uptake of mDNP or mDNP-LXR-L fluorescently labeled with FITC was monitored. A 3-fold increase in FITC mean fluorescent intensity was noted in CD11b+ macrophages isolated from atherosclerotic aortic arches from high fat high cholesterol containing WD (TD88137)-fed LDLR−/− mice treated with mDNP compared with untreated control mice (Fig 6, C) 24 or 48 hours post injection. It is noteworthy that conjugation with LXR-L did not significantly affect the overall uptake of mDNP by plaque-associated macrophages; no difference noted between the data from mice injected with mDNP and mDNP-LXR-L. To further assess the retention of mDNP by atherosclerotic plaque-associated macrophages after a single intravenous injection, CD11b+ macrophages containing FITC label from mDNP were examined by flow cytometry. As shown in Fig 6, D, the percentage of CD11b+FITC+ cells (macrophages with mDNP-FITC) in the atherosclerotic plaques was highest 3 days post intravenous injection. Although a decrease in this population of cells was noted thereafter, 20% of isolated cells were still FITC positive 8 days post injection. Collectively, these in vivo uptake data not only demonstrate successful targeting of atherosclerotic plaque-associated macrophages by mDNP but also indicate >20% retention of mDNP by the plaque-associated macrophages for at least 8 days, providing the necessary justification for a weekly treatment regimen. Furthermore, based on the observed lack of effect of mDNP administration on expression of LXR target genes in plaque-associated macrophages (Fig 7, B), no injections were given to the control group in subsequent studies.

Functionality of LXR-L delivered by mDNP-LXR-L.—To evaluate the functionality of mDNP-LXR-L in activating LXR in plaque-associated macrophages and thereby enhancing the expression of LXR target genes, expression of the specific target genes was monitored. Intravenously administered mDNP-LXR-L significantly increased the expression of ABCA1 and ABCG1 in atherosclerotic plaque-associated macrophages (Fig 7, A). Consistent with limited uptake of mDNP by hepatocytes as shown in Fig 3, B, no change in hepatic LXR target genes involved in lipogenesis (eg, FAS, SREBP-1) was observed (Fig 7, B). Therefore, mDNP represents a suitable platform for providing the beneficial effects of LXR-L at the atherosclerotic plaque site.

Lack of the undesirable hepatic effects of LXR ligand using mDNP-LXR-L.—Four weekly i.v. injections of mDNPLXR-L were given to LDLR−/− mice fed a WD for 12 weeks. Fasting plasma was collected at the time of euthanasia. Treatment with free LXR-L is reported to result in more than 2-fold increase in plasma TG and total cholesterol levels.[31] However, plasma total cholesterol or TG levels were unchanged between untreated control and mDNP-LXR-L treated mice (Fig 8, A). Although no change in the expression of FAS or SREBP1 was noted 48 hours after mDNP-LXR-L injection as shown in Fig 7, B, expression of these genes was monitored again after 4-week treatment to exclude any possible long-

term off-target effects. As shown in Fig 8, B, even after 4-week treatment, there was no increase in LXR target genes (FAS and SREBP1) in the liver. These data provide additional proof that mDNP-LXR-L represents a superior platform for the delivery of LXR-L as it eliminates the undesirable hepatic lipogenic effects. Plasma levels of aspartate transaminase and alanine transaminase remained unchanged with mDNP-LXR-L treatment, indicating lack of hepatotoxicity (Fig 8, C). Although plasma creatinine levels were below the detectible limits in control as well as mDNP-LXR-L-treated mice, BUN levels were not different between the 2 groups, suggesting no untoward renal effects (Fig 8, C). Circulating levels of interleukin-6, an inflammatory marker, were also not altered in mDNP-LXR-L-treated mice (Fig 8, C).

Modulation of atherosclerosis.—Effects of mDNP-mediated delivery of LXR-L on 2 critical parameters of atherosclerosis were monitored, namely, plaque size and inflammation. En face analyses shown in Fig 9, A, demonstrate a reduction in atherosclerotic plaques following 4-week treatment with mDNP-LXR-L, and this decrease in plaque area in the aortic arch was statistically significant (Fig 9, B). Effect of treatment on plaque development was also evaluated at another site, namely, the aortic root where plaques develop in the tricuspid aortic valve. As shown in Fig 9, C, reduced plaques were seen in mice receiving 4-week treatment with mDNP-LXR-L compared with untreated mice. Total plaque area of the aortic root or plaques in all 3 aortic valves was quantified, and percent area occupied by the plaques was significantly reduced following 4-week treatment (Fig 9, D). It should be noted that mice of both sexes were included in these studies and no significant sex-dependent differences were noted. Therefore, combined data for both sexes are presented in Fig 9, *B* and *D*. In addition to contributing to the growth and progression of atherosclerotic plaques, CE-laden macrophage foam cells also undergo increased apoptosis, leading to the development of necrotic cores. Treatment with mDNP-LXR-L not only reduced plaque area but also decreased the necrotic areas within an individual plaque (Fig 10, A). Quantification of the necrotic area as percentage of total plaque area showed a significant reduction following treatment with mDNP-LXR-L (Fig 10, B). To assess the effects of mDNP-LXR-L on the status of plaque inflammation, expression of MMP-9, an NF-κB target gene, was examined by immunohistochemistry. Dramatically reduced staining of MMP-9 was seen in plaques from mice treated with mDNP-LXR-L (Fig 11). These data are consistent with the established or direct effects of LXR activation on macrophage MMP-9 expression[42] and further demonstrate the suitability of mDNP as a strategy for delivery of anti-inflammatory agents such as LXR-L directly to the plaque site.

DISCUSSION

Targeted delivery of pharmacological agents is an actively pursued research area and a very desirable therapeutic strategy. Currently available therapies for attenuation of cardiovascular disease focus primarily on reducing plasma cholesterol with the objective of preventing plaque progression. No therapy approved for clinical use is presently available for targeted reduction in existing plaque burden or plaque-associated inflammation. Despite the demonstrated benefits of LXR activation, the undesirable hepatic lipogenic effects have precluded the use of LXR-L in vivo.[31,43] Herein we report the successful development of a

functionalized DNP-based platform (mDNP-LXR-L) for targeted delivery of LXR-L to atherosclerotic plaque-associated macrophages where *active* uptake is mediated by the presence of mannose receptor on macrophages. This is in contrast to *passive* delivery of LXR-L by PEGylated nanoparticles used before.[44] Most importantly, this functionalized platform eliminates the undesirable hepatic lipogenic effects.

Because of their well-defined structures with the near monodispersity, high water solubility, and ease of multi-functionalization, DNP represent a very attractive drug delivery platform. Three important characteristics for effective delivery using DNP are increased circulation time for enhanced uptake, specific cell targeting, and delivery of drugs such as LXR-L with limited water solubility. We introduced PEG spacers between LXR-L and PAMAM G5.0 as well as mannose and PAMAM G5.0 to accomplish longer resident time in circulation by slowing the rapid uptake of DNP by macrophages in the reticuloendothelial system. Furthermore, the zeta potential of mDNP-LXR-L decreased from ~30 mV (unmodified PAMAM dendrimer G5.0) to ~6 mV and did not change over time (Fig 2, E), suggesting that the PEGylation significantly shielded the positively charged dendrimer surface. This decreased positive charge leads to the longer circulation time and enhanced cytocompatibility of DNP. The increase in circulation time because of PEGylation and specific uptake of mDNP via the mannose receptor likely underlies the enhanced uptake and retention of mDNP-LXR-L by atherosclerotic plaque-associated macrophages out of the reticuloendothelial system. Macrophage-specific targeting of mannose-coupled nanoparticles in various tumors has been described earlier,[45–47] and mannose-functionalized PAMAM dendrimers have mainly been developed for the study of protein-carbohydrate interactions.[48] Goonewardena et al, however, demonstrated uptake of mannose-conjugated G5 dendrimers by tumor-associated macrophages as well as activated bone marrow-derived monocyte-macrophages.[49] Taking advantage of the high expression of folate receptor on activated macrophages, earlier studies have used folate functionalized nanoparticles for macrophage targeting,[50] and this strategy is currently being favorably considered for rheumatoid arthritis therapy.[51] Because of dysfunctional endothelium as well as leaky vasa vasorum, atherosclerotic plaques have high levels of exposed collagen IV that has recently been used for targeted delivery of nanoparticles to the plaque site.[52] However, whether such targeting strategies deliver the payloads specifically to plaque-associated macrophages remain to be defined. Zhang et al used PLGA-b-PEG-based nanoparticles encapsulating a synthetic LXR agonist GW 3965 for *passive* delivery to atherosclerotic plaque and did not observe an increase in hepatic expression of SREBP-1.[44] However, these studies did not involve any specific macrophage targeting, and in the absence of a demonstrated lack of altered hepatocyte uptake of PLGA-b-PEG-based nanoparticles, the authors speculated that the observed deficiency of LXR effects in the liver were likely because of accelerated clearance of these nanoparticles by hepatic sinusoids.[44] In contrast, the data presented herein directly demonstrate delivery as well as functionality of mDNP delivered LXR-L in atherosclerotic plaque-associated macrophages with no apparent increase in delivery or functionality of LXR-L in hepatocytes. Therefore, mannose functionalization represents a significant advancement over systemic delivery of LXR-L in elimination of undesirable hepatic lipogenic effects.

In addition to the plaque volume, increased cholesterol content of macrophage foam cells also contributes to increased intra-plaque inflammation, likely enhancing the necrotic processes. Large necrotic areas, considered a marker of advanced atherosclerotic lesions, are thought to destabilize the atherosclerotic plaque and induce plaque rupture that underlies acute coronary events such as heart attacks and strokes. Targeted delivery of LXR-L to plaque-associated macrophages not only reduced plaque size but also decreased necrosis. Based on the data from a genome-wide scan of LXR chromatin binding and gene regulation in human macrophages, Pehkonen et al reported a strong association with apoptosis-related functions.[53] The observed decrease in the necrotic area is, therefore, consistent with the role of LXR-L in attenuating apoptosis. Furthermore, LXR-L-dependent increase in FC efflux from plaque-associated macrophage foam cells is likely the second mechanism underlying reduced necrosis. By targeted transgenic overexpression of the rate limiting enzyme CEH in macrophages to stimulate FC efflux we have earlier demonstrated similar reduction in plaque necrosis and macrophage apoptosis.[24] Collectively, these data suggest that mDNP-LXR-L-mediated delivery of LXR-L to the plaque-associated foam cells reduces necrosis by likely enhancing FC efflux as well as reducing apoptosis.

Increased expression of MMPs and/or imbalance between MMPs and tissue inhibitor of MMPs (TIMP) results in plaque destabilization and rupture, leading to acute coronary events in humans. MMP-9 is an NF-κB target gene, and activation of LXR induces anti-inflammatory pathways including reduction in NF-κB-mediated gene expression.[28,54] Consistently, mDNP-LXR-L-mediated delivery of LXR-L resulted in dramatic reduction in the expression of MMP-9 in the plaques and is likely to contribute to plaque stability.

It needs to be emphasized that currently no treatment strategy is available to facilitate reduction in the size or volume of existing plaques; pharmacological interventions are limited to decreasing hypercholesterolemia either by reducing absorption of dietary cholesterol by ezetimibe or inhibiting de novo synthesis of cholesterol by statins. Accurate measurement of plaque volume before and after any treatment is a technical limitation in the evaluation of reduction in plaque size. Intravascular ultrasound is a recent development for in vivo assessment of plaque burden but given its invasive nature, it is currently restricted to very high-risk patients. Nonetheless, in 1 landmark study using 5 weekly injections of a reconstituted High density lipoprotein particle to enhance FC efflux from plaque-associated macrophage foam cells, reduction in plaque volume by 1.06 ± 3.17% (assessed by intravascular ultrasound) was considered clinically significant.[55] Furthermore, a recently concluded randomized controlled trial showed a 0.95% decrease in atheroma volume following treatment with proprotein convertase subtilisin kexin type 9 inhibitor evolocumab.[56] Therefore, the observed ~10% reduction in plaque area by 4 weekly injections of mDNP-LXR-L represent a promising advance, and future studies will evaluate the potential of this platform in plaque regression, provided technical advances are in place to quantify in vivo plaque burden in mice before and after treatment.

In conclusion, these preclinical studies form the basis for future development of functionalized DNP-based platforms for targeted delivery of therapeutics to be used as alternatives or in conjunction with the currently used strategies for reducing the burden of cardiovascular diseases or improving plaque stability.

ACKNOWLEDGMENTS

Conflicts of Interest: All authors have read the journal's policy on disclosure of potential conflicts of interest and have none to declare.

This work was supported in part by VCU's CTSA (UL1TR000058 from the National Institutes of Health's National Center for Advancing Translational Science) and the Center for Clinical and Translational Research (CCTR) Endowment Fund of the Virginia Commonwealth University to HY and SG as well as VA MERIT award (IO1 BX002297) to SG. HH is supported by a Post-doctoral fellowship from the American Heart Association (17POST33660608). All authors have read the journal's policy on disclosure of potential conflicts of interest and have none to declare. All authors have read the journal's authorship agreement and the manuscript has been reviewed by and approved by all named authors.

Abbreviations:

CE	cholesteryl ester
DNP	dendrimeric nanoparticles
FC	free-or unesterified cholesterol
LXR	Liver-X-receptor
mDNP	mannose functionalized DNP
mDNP-LXR-L	mDNP conjugated to LXR ligand T0901317
MPMs	mouse peritoneal macrophages
PAMAM	polyamidoamine dendrimer

REFERENCES

1. He H, Ghosh S, Yang H. Nanomedicines for dysfunctional macrophage-associated diseases. J Control Release 2017;247:106–26. [PubMed: 28057522]
2. Martinez-Pomares L The mannose receptor. J Leukoc Biol 2012;92:1177–86. [PubMed: 22966131]
3. Shen J, Hilgenbrink AR, Xia W, et al. Folate receptor-β constitutes a marker for human proinflammatory monocytes. J Leukoc Biol 2014;96:563–70. [PubMed: 25015955]
4. Miyanishi M, Tada K, Koike M, et al. Identification of tim4 as a phosphatidylserine receptor. Nature 2007;450:435–9. [PubMed: 17960135]
5. Park D, Tosello-Trampont A-C, Elliott MR, et al. Bai1 is an engulfment receptor for apoptotic cells upstream of the elmo/dock180/rac module. Nature 2007;450:430–4. [PubMed: 17960134]
6. Yi Y-S. Folate receptor-targeted diagnostics and therapeutics for inflammatory diseases. Immune Netw 2016;16:337–43. [PubMed: 28035209]
7. Zahr AS, Davis CA, Pishko MV. Macrophage uptake of core− shell nanoparticles surface modified with poly (ethylene glycol). Langmuir 2006;22:8178–85. [PubMed: 16952259]
8. Pelaz B, del Pino P, Maffre P, et al. Surface functionalization of nanoparticles with polyethylene glycol: Effects on protein adsorption and cellular uptake. ACS Nano 2015;9:6996–7008. [PubMed: 26079146]
9. Lipka J, Semmler-Behnke M, Sperling RA, et al. Biodistribution of peg-modified gold nanoparticles following intratracheal instillation and intravenous injection. Biomaterials 2010;31:6574–81. [PubMed: 20542560]
10. Holden CA, Tyagi P, Thakur A, et al. Polyamidoamine dendrimer hydrogel for enhanced delivery of antiglaucoma drugs. Nanomedicine (Lond) 2012;8:776–83.
11. Yuan Q, Yeudall WA, Yang H. Pegylated polyamidoamine dendrimers with bis-aryl hydrazone linkages for enhanced gene delivery. Biomacromolecules 2010;11:1940–7. [PubMed: 20593893]

12. Yuan Q, Lee E, Yeudall WA, Yang H. Dendrimer-triglycine-EGF nanoparticles for tumor imaging and targeted nucleic acid and drug delivery. Oral Oncol 2010;46:698–704. [PubMed: 20729136]
13. Tall AR, Yvan-Charvet L. Cholesterol, inflammation and innate immunity. Nat Rev Immunol 2015;15:104–16. [PubMed: 25614320]
14. Hendrikx T, Walenbergh S, Hofker M, Shiri-Sverdlov R. Lysosomal cholesterol accumulation: driver on the road to inflammation during atherosclerosis and non-alcoholic steatohepatitis. Obes Rev 2014;15:424–33. [PubMed: 24629059]
15. Yancey PG, St Clair R. Mechanism of the defect in cholesteryl ester clearance from macrophages of atherosclerosis-susceptible white carneau pigeons. J Lipid Res 1994;35:2114–29. [PubMed: 7897310]
16. Rothblat G, De La Llera-Moya M, Favari E, Yancey P, Kellner-Weibel G. Cellular cholesterol flux studies: methodological considerations. Atherosclerosis 2002;163:1–8. [PubMed: 12048116]
17. Ghosh S, Clair RWS, Rudel LL. Mobilization of cytoplasmic CE droplets by overexpression of human macrophage cholesteryl ester hydrolase. J Lipid Res 2003;44:1833–40. [PubMed: 12837853]
18. Zhao B, Song J, Clair RWS, Ghosh S. Stable overexpression of human macrophage cholesteryl ester hydrolase results in enhanced free cholesterol efflux from human thp1 macrophages. Am J Physiol Cell Physiol 2007;292:C405–12. [PubMed: 16971496]
19. He H, Lancina MG, Wang J, et al. Bolstering cholesteryl ester hydrolysis in liver: a hepatocyte-targeting gene delivery strategy for potential alleviation of atherosclerosis. Biomaterials 2017;130:1–13. [PubMed: 28349866]
20. Wang N, Lan D, Chen W, Matsuura F, Tall AR. ATP-binding cassette transporters g1 and g4 mediate cellular cholesterol efflux to high-density lipoproteins. Proc Natl Acad Sci USA 2004;101:9774–9. [PubMed: 15210959]
21. Joyce CW, Amar MJ, Lambert G, et al. The ATP binding cassette transporter a1 (ABCA1) modulates the development of aortic atherosclerosis in c57bl/6 and apoE-knockout mice. Am J Physiol Cell Physiol 2002;99:407–12.
22. Singaraja RR, Fievet C, Castro G, et al. Increased abca1 activity protects against atherosclerosis. J Clin Invest 2002;110:35–42. [PubMed: 12093886]
23. Aiello RJ, Brees D, Bourassa P-A, et al. Increased atherosclerosis in hyperlipidemic mice with inactivation of abca1 in macrophages. Arterioscler Thromb Vasc Biol 2002;22:630–7. [PubMed: 11950702]
24. Zhao B, Song J, Chow WN, et al. Macrophage-specific transgenic expression of cholesteryl ester hydrolase significantly reduces atherosclerosis and lesion necrosis in Ldlr–/–mice. J Clin Invest 2007;117:2983–92. [PubMed: 17885686]
25. Oram JF, Heinecke JW. Atp-binding cassette transporter a1: a cell cholesterol exporter that protects against cardiovascular disease. Physiol Rev 2005;85:1343–72. [PubMed: 16183915]
26. Joseph SB, Tontonoz P. LXRs: new therapeutic targets in atherosclerosis? Curr Opin Pharmacol 2003;3:192–7. [PubMed: 12681243]
27. Ghosh S, Zhao B, Bie J, Song J. Macrophage cholesteryl ester mobilization and atherosclerosis. Vascul Pharmacol 2010;52:1–10. [PubMed: 19878739]
28. Zelcer N, Tontonoz P. Liver x receptors as integrators of metabolic and inflammatory signaling. J Clin Invest 2006;116:607–14. [PubMed: 16511593]
29. Joseph SB, McKilligin E, Pei L, et al. Synthetic LXR ligand inhibits the development of atherosclerosis in mice. Proc Natl Acad Sci USA 2002;99:7604–9. [PubMed: 12032330]
30. Tangirala RK, Bischoff ED, Joseph SB, et al. Identification of macrophage liver x receptors as inhibitors of atherosclerosis. Proc Natl Acad Sci USA 2002;99:11896–901. [PubMed: 12193651]
31. Schultz JR, Tu H, Luk A, et al. Role of LXRs in control of lipogenesis. Genes Dev 2000;14:2831–8. [PubMed: 11090131]
32. Cha J-Y, Repa JJ. The liver x receptor (LXR) and hepatic lipogenesis the carbohydrate-response element-binding protein is a target gene of LXR. J Biol Chem 2007;282:743–51. [PubMed: 17107947]

33. Yang H, Kao WJ. Synthesis and characterization of nanoscale dendritic RGD clusters for potentialapplications in tissue engineering and drug delivery. Int J Nanomedicine 2007;2:89. [PubMed: 17722516]
34. McIntyre JO, Scherer RL, Matrisian LM. Near-infrared optical proteolytic beacons for in vivo imaging of matrix metalloproteinase activity. Methods Mol Biol 2010;622:279–304. [PubMed: 20135290]
35. Yang H, Morris JJ, Lopina ST. Polyethylene glycol–polyamidoamine dendritic micelle as solubility enhancer and the effect of the length of polyethylene glycol arms on the solubility of pyrene in water. J Colloid Interface Sci 2004;273:148–54. [PubMed: 15051444]
36. Hylemon P, Gurley E, Kubaska W, et al. Suitability of primary monolayer cultures of adult rat hepatocytes for studies of cholesterol and bile acid metabolism. J Biol Chem 1985;260:1015–9. [PubMed: 3968056]
37. Hajjar D, Minick CR, Fowler S. Arterial neutral cholesteryl esterase. A hormone-sensitive enzyme distinct from lysosomal cholesteryl esterase. J Biol Chem 1983;258:192–8. [PubMed: 6848493]
38. Ghosh S, Grogan WM. Activation of rat liver cholesterol ester hydrolase by camp-dependent protein kinase and protein kinase c. Lipids 1989;24:733–6. [PubMed: 2555647]
39. Galkina E, Kadl A, Sanders J, et al. Lymphocyte recruitment into the aortic wall before and during development of atherosclerosis is partially l-selectin dependent. J Exp Med 2006;203:1273–82. [PubMed: 16682495]
40. Bie J, Zhao B, Ghosh S. Atherosclerotic lesion progression is attenuated by reconstitution with bone marrow from macrophage-specific cholesteryl ester hydrolase transgenic mice. Am J Physiol Regul Integr Comp Physiol 2011;301:R967–74. [PubMed: 21795638]
41. Linehan SA. The mannose receptor is expressed by subsets of APC in non-lymphoid organs. BMC Immunol 2005;6:4. [PubMed: 15701168]
42. Castrillo A, Joseph SB, Marathe C, Mangelsdorf DJ, Tontonoz P. Liver x receptor-dependent repression of matrix metalloproteinase-9 expression in macrophages. J Biol Chem 2003;278:10443–9. [PubMed: 12531895]
43. Joseph SB, Laffitte BA, Patel PH, et al. Direct and indirect mechanisms for regulation of fatty acid synthase gene expression by liver x receptors. J Biol Chem 2002;277:11019–25. [PubMed: 11790787]
44. Zhang XQ, Even-Or O, Xu X, et al. Nanoparticles containing a liver x receptor agonist inhibit inflammation and atherosclerosis. Adv Healthc Mater 2015;4:228–36. [PubMed: 25156796]
45. Zhu S, Niu M, O'Mary H, Cui Z. Targeting of tumor-associated macrophages made possible by PEG-sheddable, mannose-modified nanoparticles. Mol Pharm 2013;10:3525–30. [PubMed: 23901887]
46. Byeon HJ, Lee S, Min SY, et al. Doxorubicin-loaded nanoparticles consisted of cationic-and mannose-modified-albumins for dual-targeting in brain tumors. J Control Release 2016;225: 301–13. [PubMed: 26826308]
47. He C, Yin L, Tang C, Yin C. Multifunctional polymeric nanoparticles for oral delivery of TNF-α siRNA to macrophages. Biomaterials 2013;34:2843–54. [PubMed: 23347838]
48. Samuelson LE, Sebby KB, Walter ED, Singel DJ, Cloninger MJ. EPR and affinity studies of mannose–TEMPO functionalized PAMAM dendrimers. Org Biomol Chem 2004;2:3075–9. [PubMed: 15505710]
49. Goonewardena SN, Zong H, Leroueil PR, Baker JR. Bioorthogonal chemical handle for tracking multifunctional nanoparticles. Chempluschem 2013;78:430–7.
50. Zhao X, Li H, Lee RJ. Targeted drug delivery via folate receptors. Expert Opin Drug Deliv 2008;5:309–19. [PubMed: 18318652]
51. Nogueira E, Gomes AC, Preto A, Cavaco-Paulo A. Folate-targeted nanoparticles for rheumatoid arthritis therapy. Nanomedicine (Lond) 2016;12:1113–26.
52. Kamaly N, Fredman G, Fojas JJR, et al. Targeted interleukin-10 nanotherapeutics developed with a microfluidic chip enhance resolution of inflammation in advanced atherosclerosis. ACS Nano 2016;10:5280–92. [PubMed: 27100066]

53. Pehkonen P, Welter-Stahl L, Diwo J, et al. Genome-wide landscape of liver x receptor chromatin binding and gene regulation in human macrophages. BMC Genomics 2012;13:50. [PubMed: 22292898]

54. Ogawa S, Lozach J, Benner C, et al. Molecular determinants of crosstalk between nuclear receptors and toll-like receptors. Cell 2005;122:707–21. [PubMed: 16143103]

55. Nissen SE, Tsunoda T, Tuzcu EM, et al. Effect of recombinant ApoA-I Milano on coronary atherosclerosis in patients with acute coronary syndromes: a randomized controlled trial. JAMA 2003;290:2292–300. [PubMed: 14600188]

56. Nicholls SJ, Puri R, Anderson T, et al. Effect of evolocumab on progression of coronary disease in statin-treated patients: the GLAGOV randomized clinical trial. JAMA 2016;316:2373–84. [PubMed: 27846344]

AT A GLANCE COMMENTARY

Background

No modalities are currently available to directly deliver therapeutic agents to atherosclerotic plaque-associated dysfunctional macrophages to modulate plaque size or characteristics. Herein, we describe the development of a mannose-functionalized dendrimeric nanoparticle platform for specific delivery of LXR ligand to plaque-associated macrophages. In contrast to increased hepatic lipogenesis associated with systemic delivery of LXR ligands, no dyslipidemia was noted while athero-sclerotic plaque size as well as plaque inflammation or necrosis was reduced.

Translational Significance

Development of a macrophage-specific delivery platform represents a significant advance in direct delivery of pharmaceutical agents to atherosclerotic plaque-associated macrophages to beneficially modulate disease process and improve outcomes.

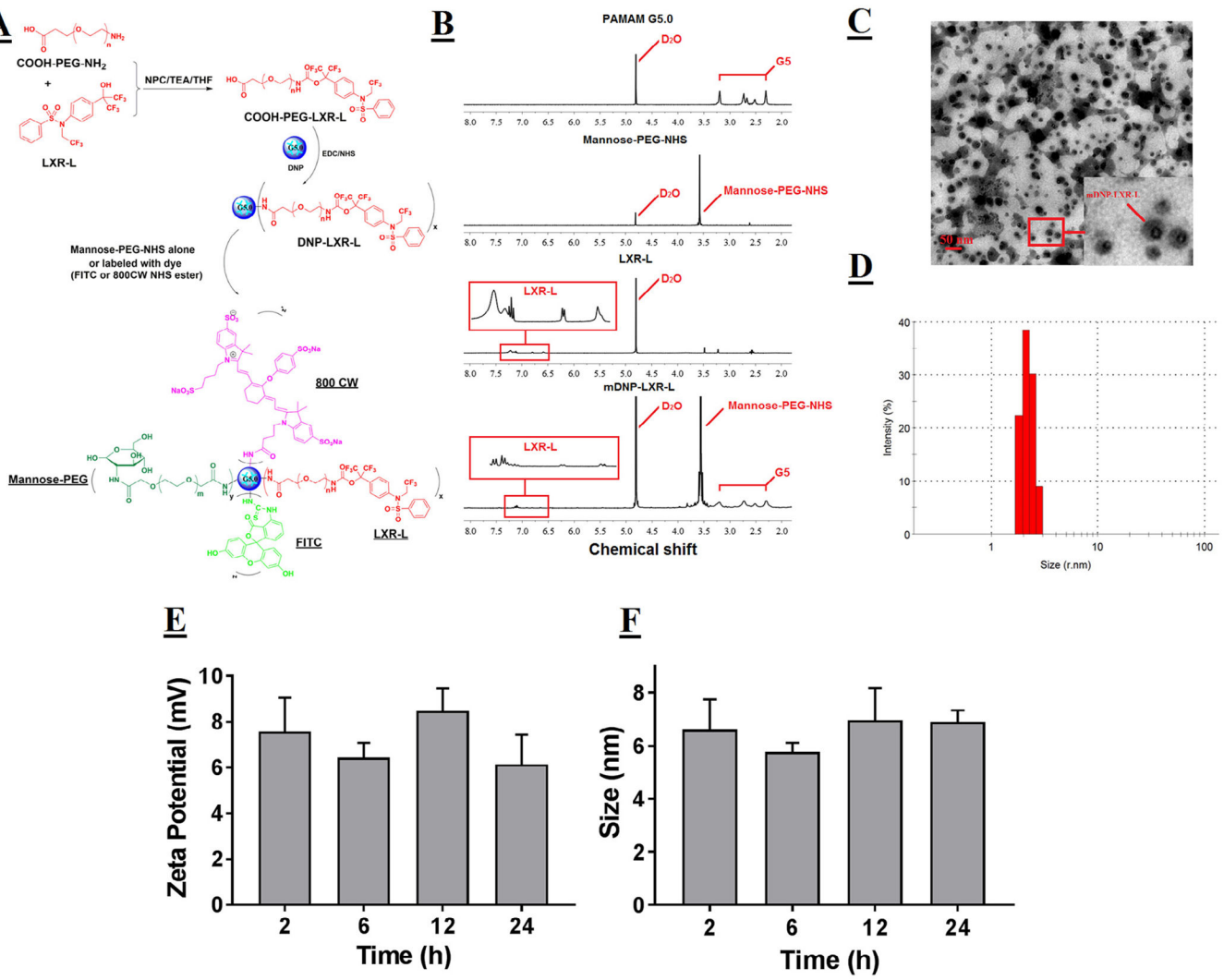

Fig 1.

Synthesis and characterization of mDNP-LXR-L. (**A**) Schematic to show the steps involved in the synthesis. LXR-L was PEGylated and then coupled with DNP G5.0 to form DNP-LXR-L. Mannose-PEG-NHS was conjugated with DNP-LXR-L to get mDNP-LXR-L. To facilitate in vitro and in vivo imaging, mDNP-LXR-L was labeled with either FITC or 800CW. (**B**) The 300 MHz ^{1}H NMR spectrum of pure PAMAM G5, mannose-PEG-NHS, LXR-L, and mDNP-LXR-L. In the spectrum of mDNP-LXR-L, multiple protons peaks between 2.2 and 3.4 ppm belong to protons from PAMAM G5; a singlet peak at 3.6 ppm belongs to the repeat units of PEG in mannose-PEG-NHS and peaks in the red rectangle stand for the LXR-L. (**C**) Morphology of mDNP-LXR-L visualized by TEM. (**D**) Hydrodynamic size of mDNP-LXR-L measured by DLS. (**E**) Changes on zeta potential of mDNP-LXR-L in colloidal state over 24 hours. (**F**) Changes on size of mDNP-LXR-L in colloidal state over 24 hours. DLS, Differential light scattering; FITC, fluorescein isothiocyanate; LXR-L, liver-x-receptor ligand; mDNP, mannose-functionalized dendrimeric nanoparticles; NHS, N-hydroxysuccinimide; NMR, Nuclear Magnetic Resonance; PAMAM, polyamidoamine dendrimer; TEM, Transmission Electron Microscopy.

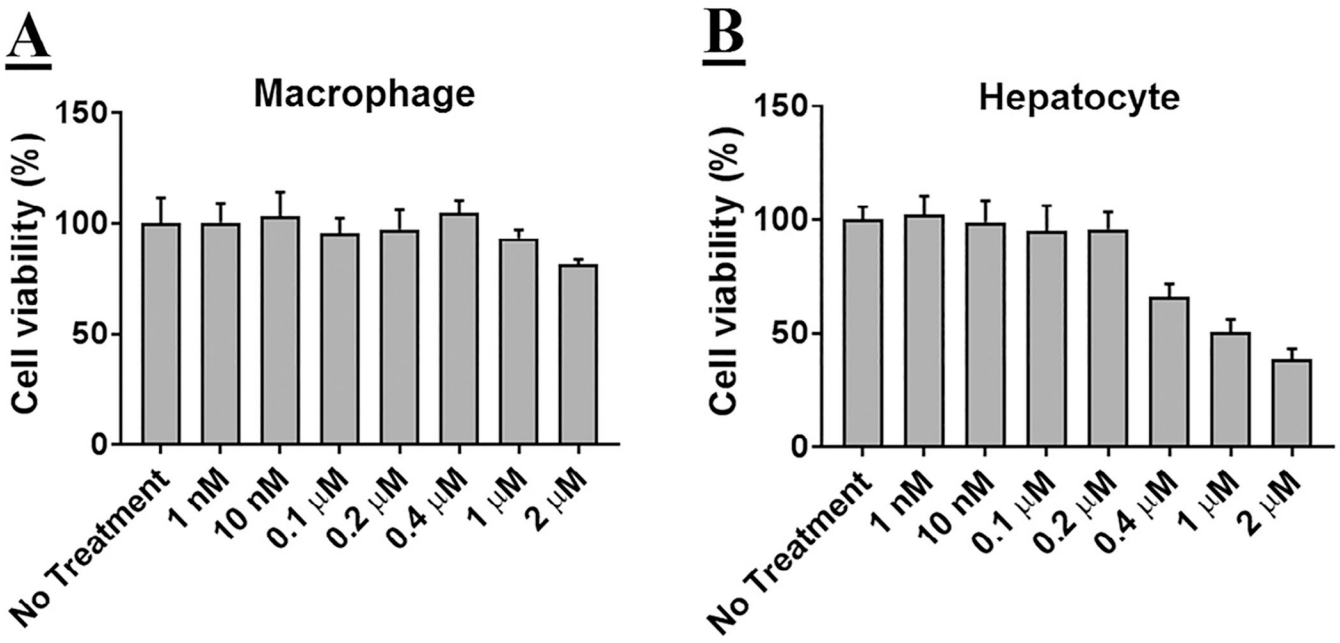

Fig 2.

mDNP-LXR-L does not affect cell viability: (**A**) Freshly isolated MPMs (0.8×10^6 cells/well) were plated in 48-well plates and growth medium was changed after 4 hours. After 24 hours, the growth medium was replaced with fresh medium containing increasing concentrations of mDNP-LXR-L and incubated for additional 24 hours. Cell viability was determined using WST-1 assay. (**B**) Freshly isolated hepatocytes (0.3×10^6 cells/well) were plated in 48-well plates, and growth medium was changed after 4 hours. After 24 hours, the growth medium was replaced with fresh medium containing increasing concentrations of mDNP-LXR-L and incubated for additional 24 hours. Cell viability was determined using WST-1 assay. Data are expressed as % cell viability compared with the no treatment control (mean ± SD, n = 6). LXR L, liver-x-receptor ligand; mDNP, mannose-functionalized dendrimeric nanoparticles; MPM, mouse peritoneal macrophages; WST-1, Water soluble tetrazolium-1.

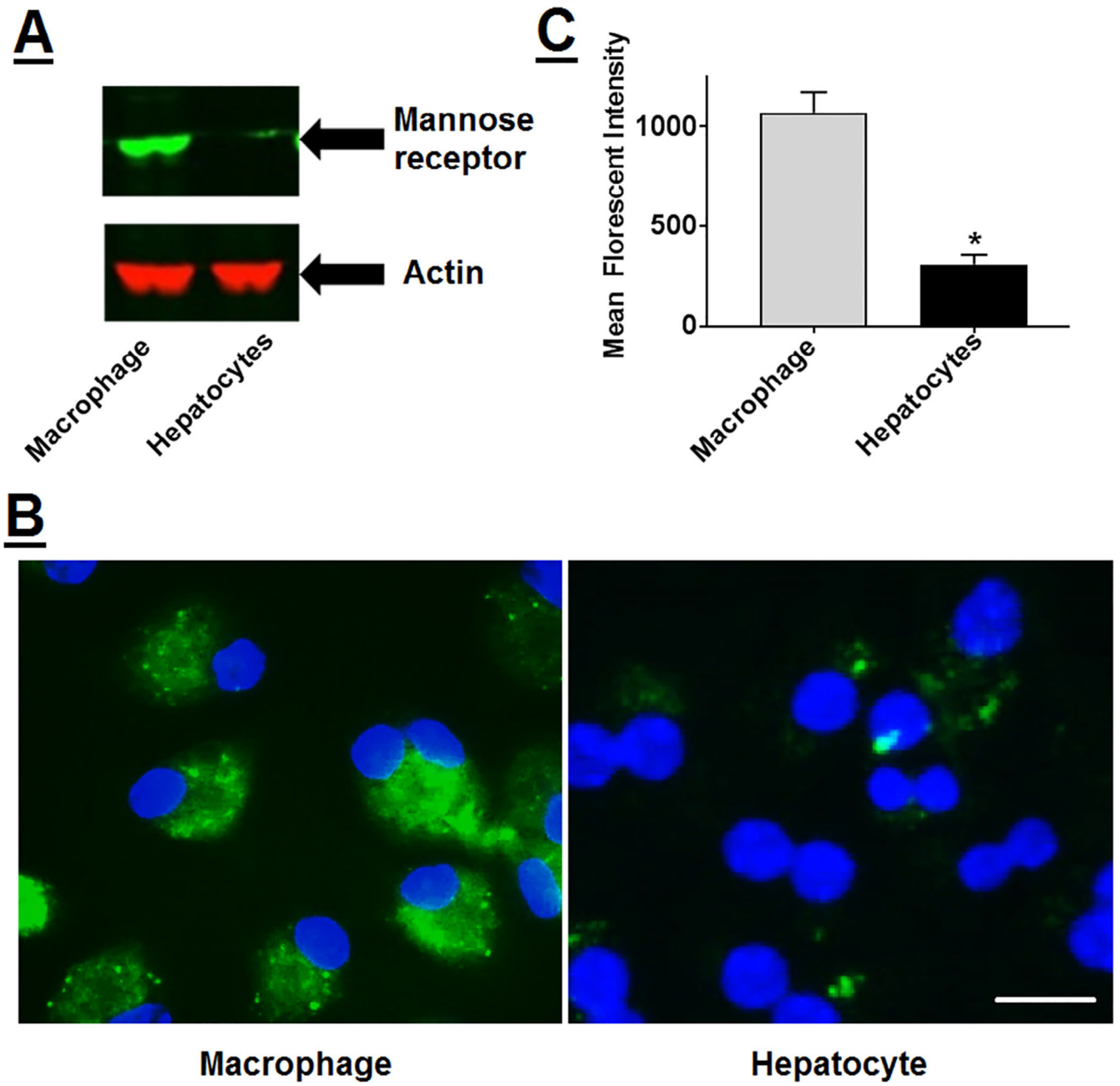

Fig 3.

Specific uptake of mDNP-FITC by macrophages: (**A**) Total protein extracts prepared from freshly isolated MPMs as well as primary mouse hepatocytes were subjected to Western blot analyses to evaluate the expression of mannose receptor. Blots were stripped and reprobed with β-actin as the housekeeping gene. (**B**) MPMs as well as hepatocytes were plated in 2-well chamber slides as described under Methods section and incubated with mDNPFITC (0.2 μM) for 24 hours. Cells were washed with PBS, fixed with buffered formalin, and imaged using Carl Zeiss inverted fluorescent microscope. (**C**) MPMs as well as hepatocytes were plated in 6-well tissue culture dishes and incubated with mDNP-FITC (0.2 μM). After

24 hours, cells were harvested and cell-associated FITC fluorescence was determined by FACS. Data (mean ± SD, n = 6) are shown as mean fluorescent intensities. FACS, Fluorescence activated cell sorting; FITC, fluorescein isothiocyanate; mDNP, mannose-functionalized dendrimeric nanoparticles; MPM, mouse peritoneal macrophages; PBS, phosphate-buffered saline.

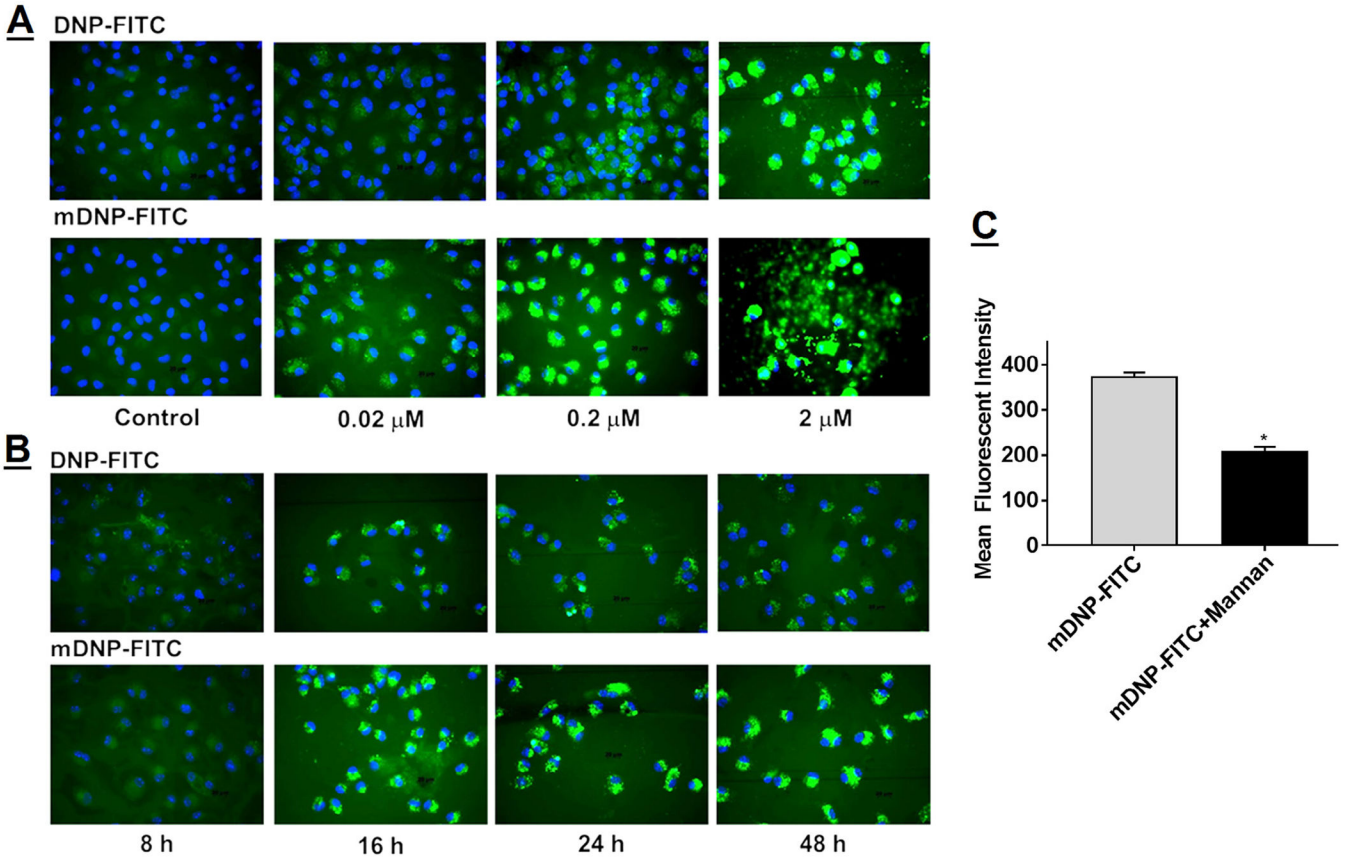

Fig 4.

Concentration- and time-dependent increase in the uptake of mDNP-FITC by MPMs. (**A**) Freshly isolated MPMs were plated in 2-well chamber slides and incubated with increasing concentration of either FITC (green)-labeled DNP (DNP-FITC) or with FITC-labeled mannose functionalized DNP (mDNP-FITC) for 24 hours. (**B**) Freshly isolated MPMs were plated in 2-well chamber slides and incubated with 0.2 μM of either DNP-FITC or with mDNP-FITC for 8–48 hours, as indicated. Cells were washed with PBS, permeabilized, counterstained with nuclear stain DAPI (blue), and imaged as described under Methods section. Representative images from 3 independent experiments are shown. (**C**) MPMs were plated in 24-well plates and incubated with mDNP-FITC (0.2 μM) in the absence or presence of mannose receptor antagonist, mannan (0.1 mM). After 24 hours, the cells were harvested and cell-associated FITC fluorescence was determined by FACS. Data (mean ± SD, n = 6) are shown as mean fluorescent intensities. DAPI, 4’, 6-diamino-2-phenylindole; FACS, Fluorescence activated cell sorting; FITC, fluorescein isothiocyanate; mDNP, mannosefunctionalized dendrimeric nanoparticles; MPM, mouse peritoneal macrophages; PBS, phosphate-buffered saline.

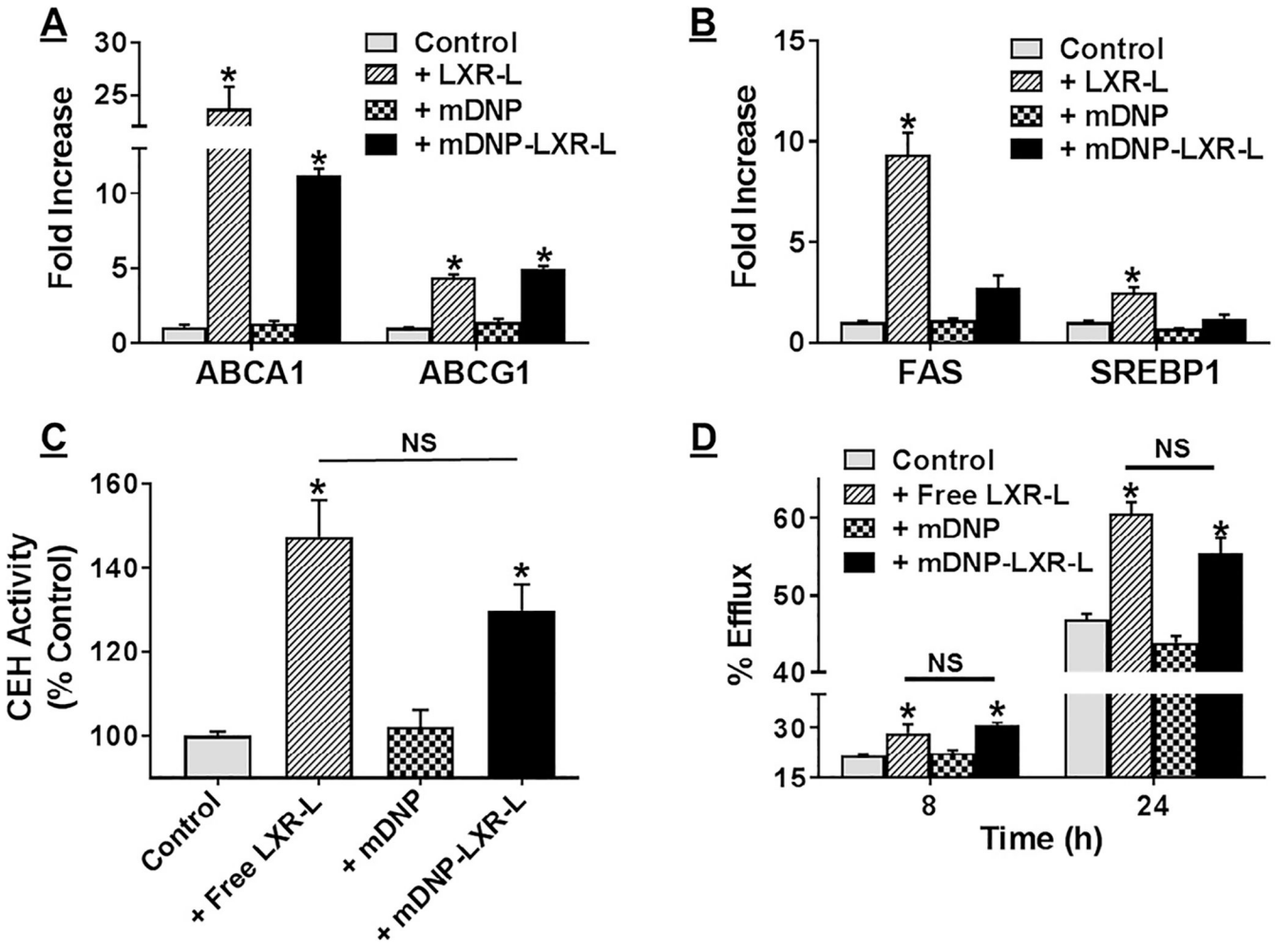

Fig 5.

mDNP-LXR-L delivered LXR ligand appropriately increases gene expression leading to increased FC efflux. MPMs (**A**) or primary hepatocytes (**B**) were plated in 6-well culture dishes and incubated with either LXR ligand T0901317 or mDNP or mDNP-LXR-L (0.2 ^CM) for 24 hours; untreated cells were used as controls. Expression of LXR target genes (ABCA1 and ABCG1 in MPMs and FAS and SREBP1 in hepatocytes) was evaluated by QPCR using total RNA as described under Methods section. Data (mean ± SD, n = 3) are expressed as fold increase over controls. (**C**) MPMs e plated in 6-well plates were exposed to either LXR ligand T0901317 or mDNP or mDNP-LXR-L (0.2 μM) for 24 hours. Cells were washed once with cold PBS and harvested in cold buffer on ice as described under Methods section. Following disruption of cells by sonication and removal of cell debris, CEH activity was measured using a radiometric assay. CEH activity (mean ± SD, n = 3) is expressed as % untreated controls. (**D**) MPMs, plated in 24-well plate, were loaded and labeled with [^{3}H]-cholesterol as described under Methods section. During the 24 hours equilibration, cells were exposed to either LXR ligand T0901317 or mDNP or mDNP-LXR-L (0.2 μM). FC efflux to medium containing 10% FBS was monitored for 8 and 24 hours. Data (mean ± SD, n = 6) are expressed as % efflux. *$P < 0.05$ and NS—not significant. CEH, cholesteryl esters hydrolase; FBS, fetal bovine serum; LXRL, liver-x-receptor ligand;

mDNP, mannose-functionalized dendrimeric nanoparticles; MPM, mouse peritoneal macrophages; PBS, phosphate-buffered saline; QPCR, quantitative or real-time polymerase chain reaction.

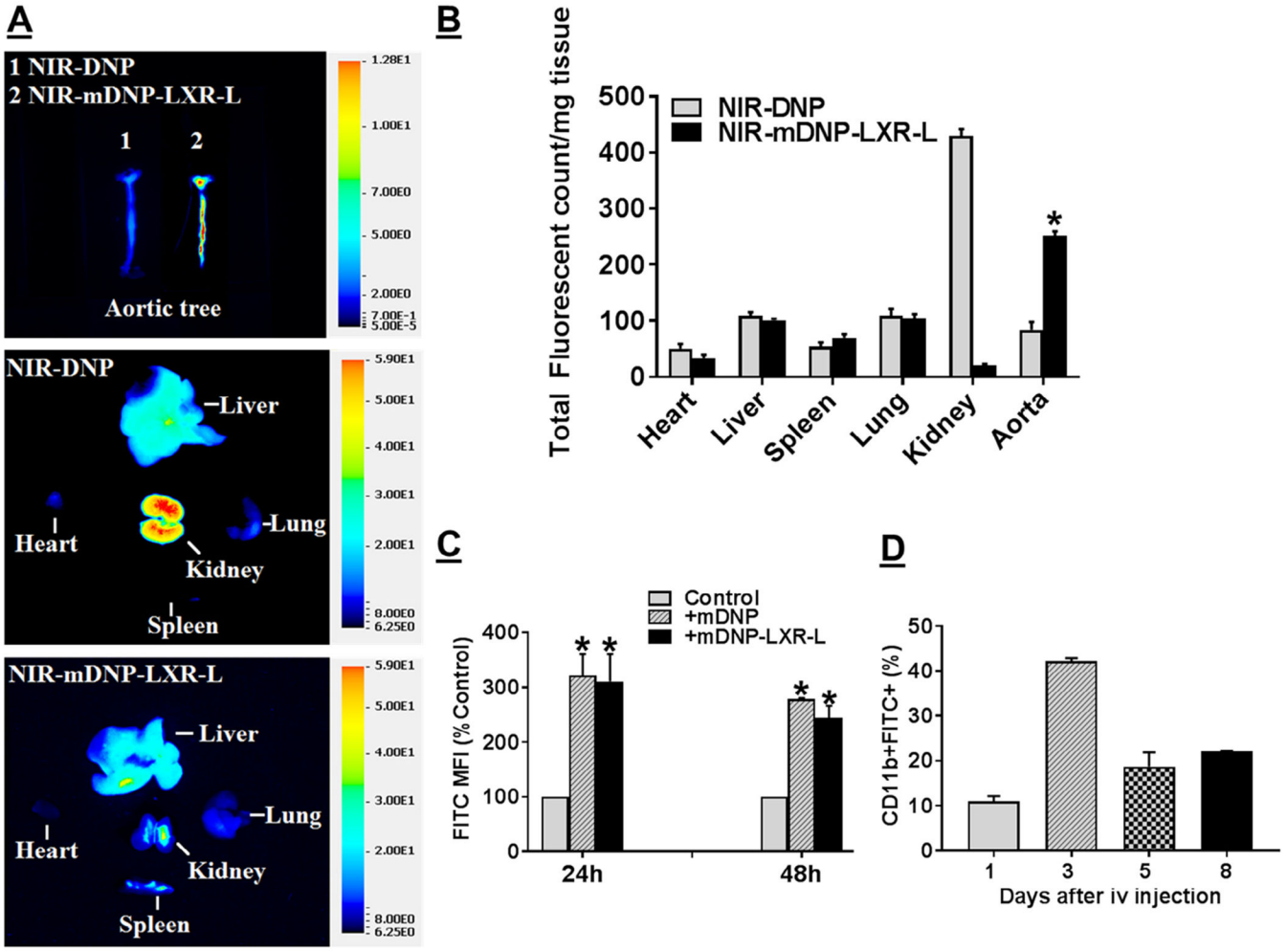

Fig 6.

In vivo uptake of mDNP by tissues and arterial plaque-associated macrophages: LDLR−/− mice (both sexes) with established atherosclerotic plaques were injected (i.v.) with either NIR-DNP or NIR-mDNP-LXR-L in sterile PBS. (**A** and **B**) After 24 hours, mice were euthanized, and major organs (heart, liver, spleen, lung, and kidney) as well as entire aorta from the heart to the iliary bifurcation was removed and cleaned to remove all the adventitious tissue. After opening to expose the arterial plaques, the aortas were imaged to assess uptake of fluorescent mDNP. Representative images are shown in A and quantification is shown in **B**. Data (mean ± SD, n = 6) are presented as total fluorescence per milligram tissue. (**C**) For assessing the uptake of mDNP-FITC by aortic plaque-associated macrophages, Western diet-fed LDLR−/− mice were either injected with PBS, or mDNP-FITC or mDNP-LXR-L-FITC. Control animals were injected with PBS alone. Following euthanasia after 24 or 48 hours, aortic arch from each mouse was quickly dissected and digested to obtain single cell suspension as described under Methods section. Cells were then stained for CD11b and analyzed by flow cytometry. Mean fluorescent Intensity, a measure of FITC-labeled DNP uptake is shown as % control (mean ± SD, n = 4). *$P < 0.05$. (**D**) In a separate experiment, time-dependent retention of FITC-labeled mDNP-LXLR-L by atherosclerotic plaque-associated macrophages after a single i.v. injection was monitored.

Data (mean ± SD, n = 3) are shown as % of CD11b+FITC+ cells in the total cells isolated. FITC, fluorescein isothiocyanate; LXR-L, liver-x-receptor ligand; mDNP, mannose-functionalized dendrimeric nanoparticles; NIR, Near infrared.

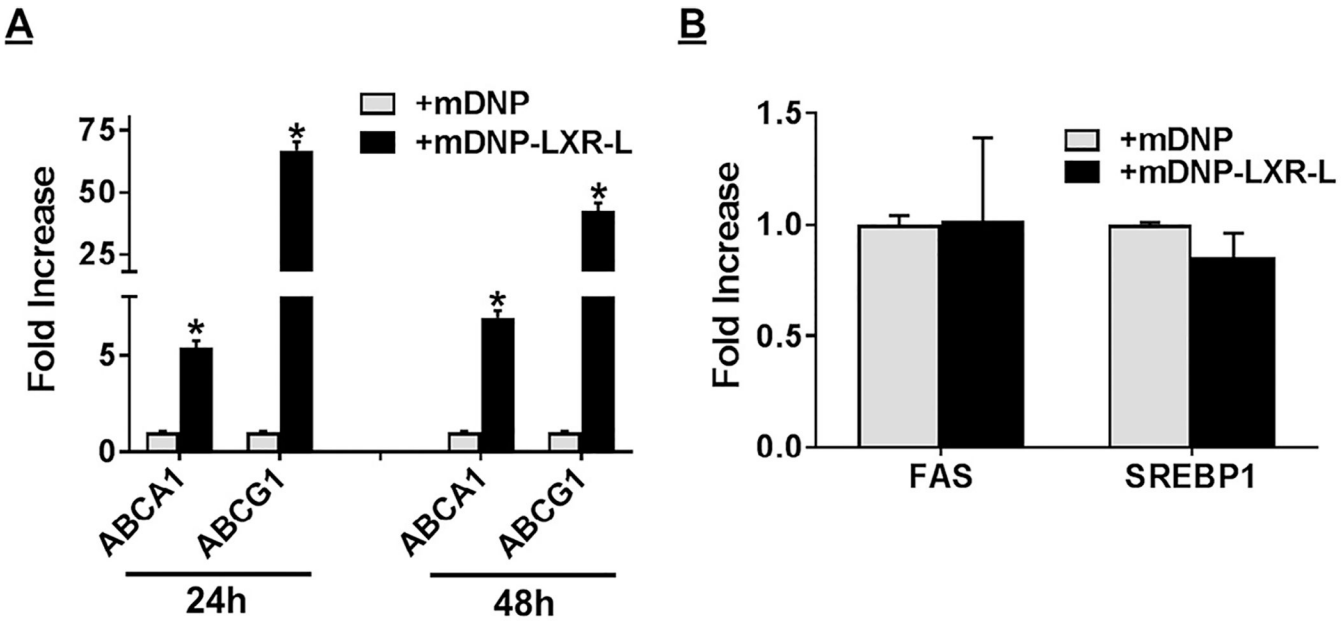

Fig 7.

Delivery of LXR ligand using mDNP-LXR-L increases expression of LXR target genes in plaque-associated macrophages but does not affect expression of lipogenic genes in the liver. Mannose functionalized DNP (mDNP) with or without conjugated LXR ligand in sterile PBS were injected via the tail vein of LDLR−/− atherosclerotic mice of both sexes. Control animals were injected with PBS alone. Following euthanasia, aortic arch and liver from each mouse was quickly dissected and total RNA was isolated. Gene expression of the indicated genes in aortic arch associated macrophages (**A**) and liver (**B**) was assessed by QPCR as described under Methods section. Data (mean ± SD, n = 3) are expressed as fold increase over controls. **P* < 0.05. LXR, liver-x-receptor; mDNP, mannose-functionalized dendrimeric nanoparticles; PBS, phosphate-buffered saline; QPCR, Quantitative or real-time polymerase chain reaction.

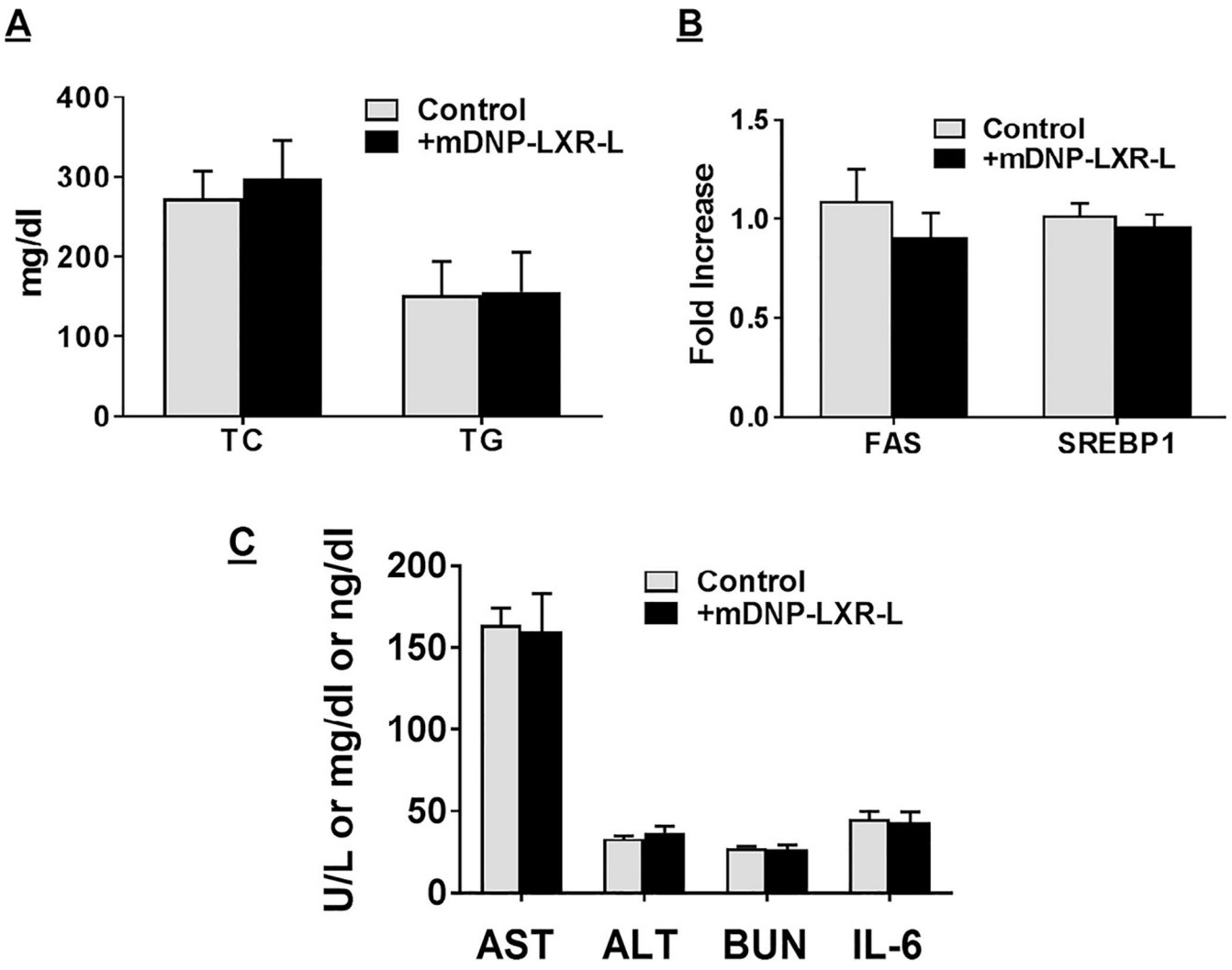

Fig 8.

Specific delivery of LXR ligand by mDNP-LXR-L does not affect plasma lipid composition and hepatic gene expression. Atherosclerotic LDLR−/− mice of both sexes were given 4 weekly i.v. injections of mDNP-LXR-L. Plasma and liver were collected at the time of euthanasia and analyzed as described under Methods section. (**A**) Plasma total cholesterol (TC) and triglyceride (TG) levels are shown as mg/dL (mean ± SD, n = 6). (**B**) Expression (relative to untreated controls) of indicated genes in liver was determined and data are presented as mean ± SD, n = 6. (**C**) Plasma levels of AST, ALT (U/L), BUN (mg/dL), and IL-6 (ng/dL) and data are presented as mean ± SD, n = 6. ALT, alanine transaminase; BUN, blood urea nitrogen; IL-6, Interleukin-6; LXR-L, liver-x-receptor ligand; mDNP, mannose-functionalized dendrimeric nanoparticles.

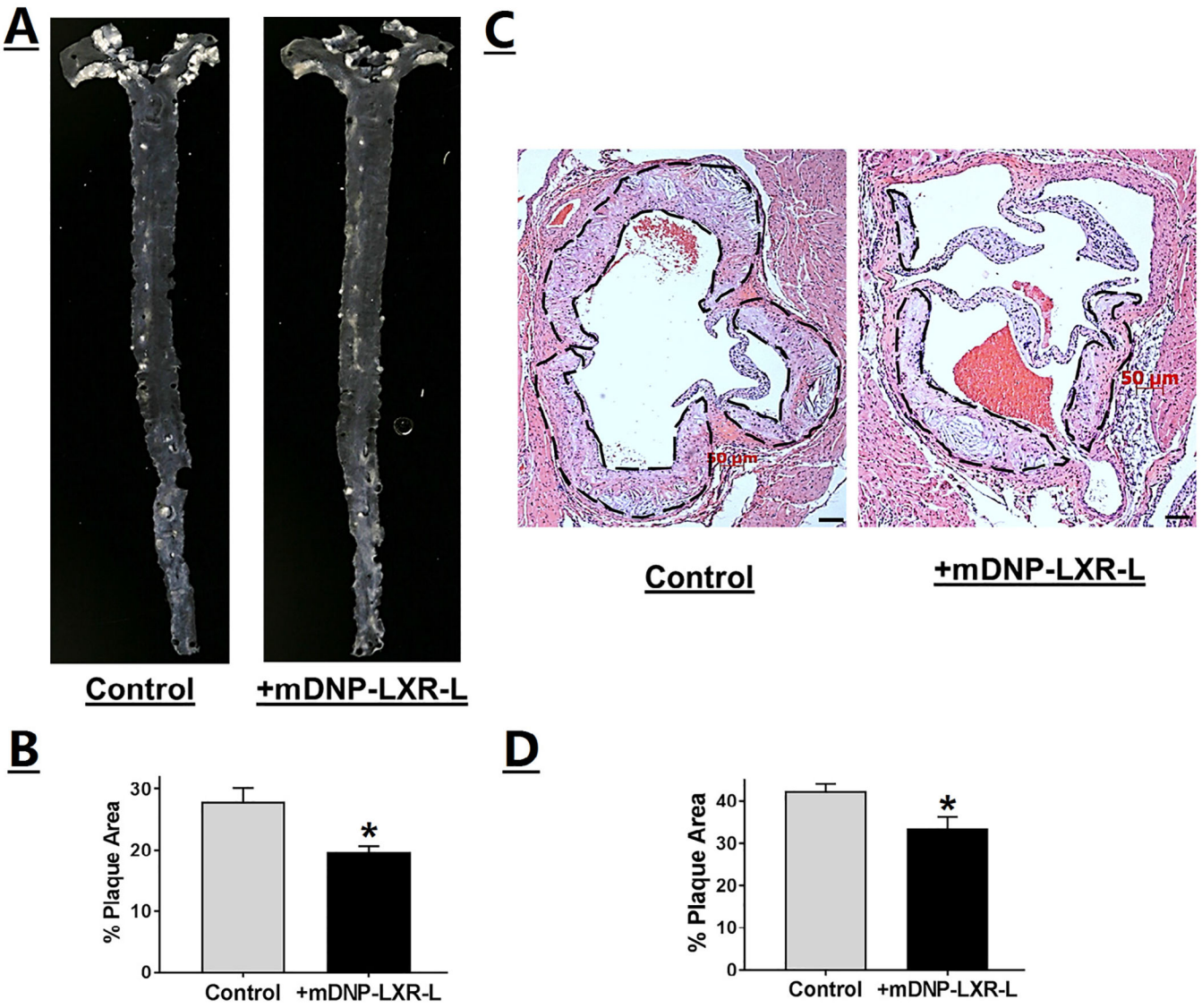

Fig 9.

Specific delivery of LXR ligand by mDNP-LXR-L attenuates plaque development. LDLR−/− mice were fed a Western-type high-fat high-cholesterol diet for 12 weeks and divided into 2 experimental groups, and received weekly injections of either PBS (control) or mDNP-LXR-L (200 μg in 100 μL sterile PBS, labeled treated) via the tail vein. Mice were euthanized after 4 weeks of treatment. (**A**) Representative en face images of the aortas. (**B**) Quantification of the area occupied by the plaque in the aortic arch (white opaque areas in the images) was performed using Axiovision software and the data are presented as % plaque area (mean ± SD, n = 6, both sexes). (**C**) Hearts were fixed in buffered formalin, embedded in paraffin, and 5-μm sections were stained with H&E. Images were acquired using Carl Zeiss inverted microscope. Representative images of the aortic root showing the plaque development in the aortic valve leaflets (marked by black dashed lines). (**D**) Quantification of the plaque area. Data are expressed as % plaque area per leaflet (mean ± SD, n = 6, both genders). **P* < 0.05. H&E, hematoxylineosin; LXR-L, liver-x-receptor

ligand; mDNP, mannose-functionalized dendrimeric nanoparticles; PBS, phosphate-buffered saline.

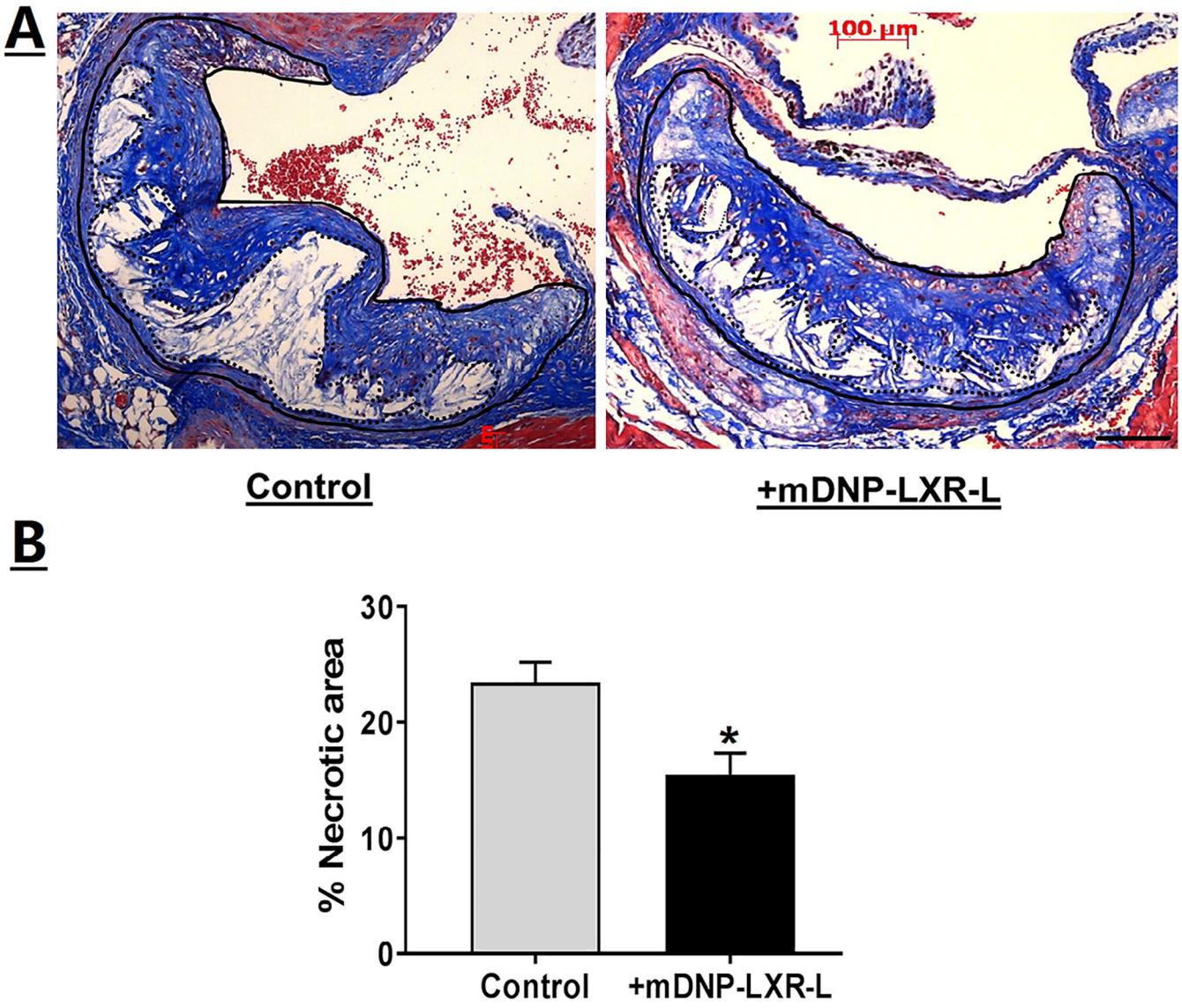

Fig 10.

Specific delivery of LXR ligand by mDNP-LXR-L attenuates plaque necrosis. (**A**) Serial sections (5 µm) of the aortic root from paraffin-embedded hearts (from mice described in Fig 9) were stained with Mason's trichrome stain. Images were acquired using Carl Zeiss inverted microscope. Representative images of the aortic root showing the necrotic areas (white blank areas) in the aortic valve leaflets. (**B**) Quantification of the necrotic area. Total plaque was outlined (solid black line) and necrotic white areas were identified using Axiovision software (shown by dotted line) and % necrotic area calculated. Data are expressed as % necrotic area per plaque (mean ± SD, n = 9). **P* < 0.05. LXR-L, liver-x-receptor ligand; mDNP, mannose-functionalized dendrimeric nanoparticles

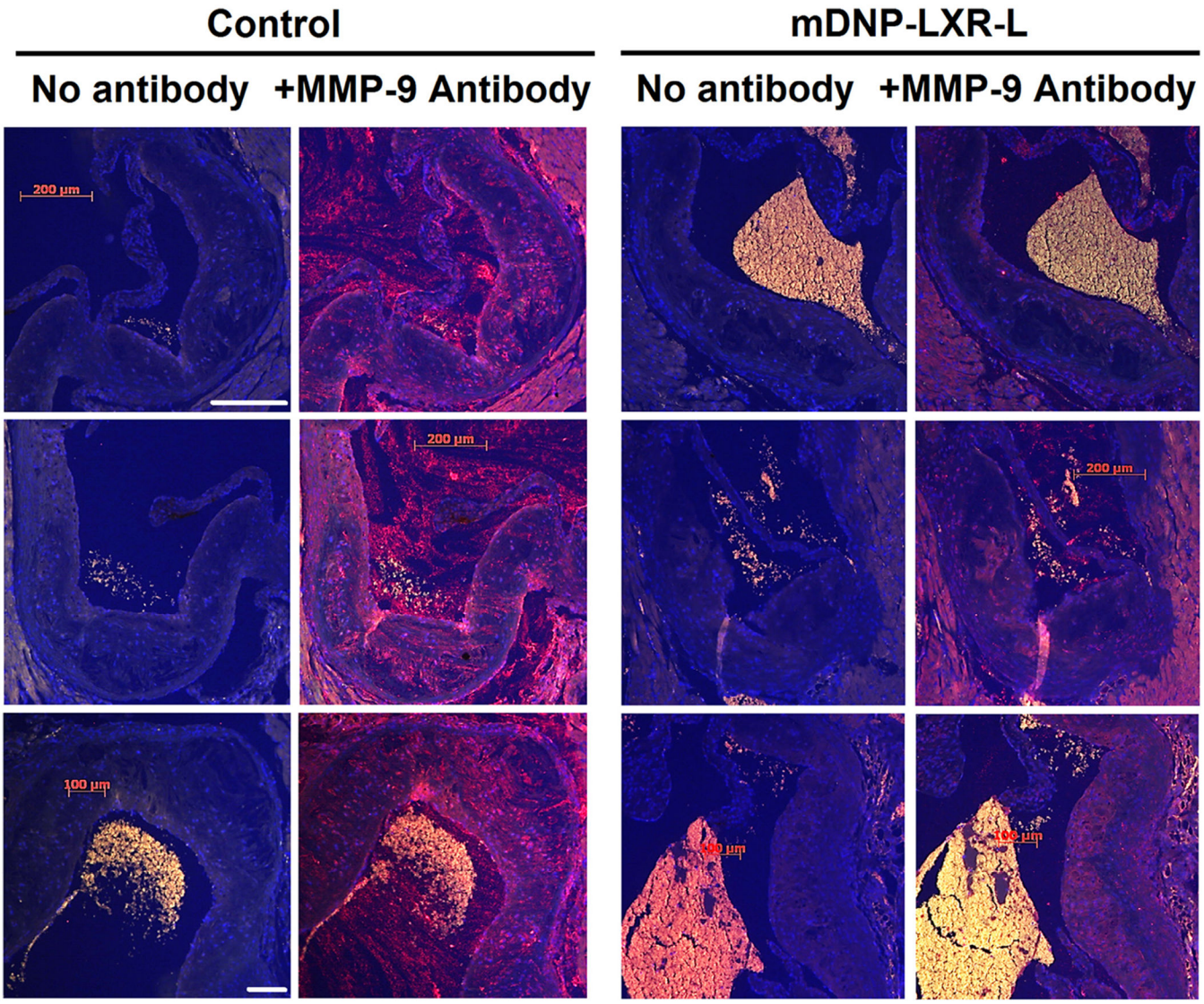

Fig 11.

Specific delivery of LXR ligand by mDNP-LXR-L attenuates expression of pro-inflammatory and NF-κB target gene MMP-9. Serial sections (5 µm) of the aortic root from mice described in Fig 9 (n = 6) were stained for MMP-9 as described under Methods section; specificity of MMP-9 staining was confirmed by staining the sections in the absence of MMP-9 antibody (labeled—No antibody). Images were acquired using Carl Zeiss inverted microscope under same exposure parameters. Three representative images for each condition are shown. Control—heart sections from mice with no i.v. injections; +mDNP-LXR-L—Heart sections from mice given 4 weekly injections of mDNP-LXR-L. LXR-L, liver-x-receptor ligand; mDNP, mannose-functionalized dendrimeric nanoparticles; MMP, matrix metalloproteinase; NF-κB, nuclear factor kappa B.